OPEN ACCESS

Chemical Biology ARTICLE

The Innovation Drug Discovery

Discovery of a highly selective JAK3 inhibitor for the treatment of inflammatory bowel disease

Caolin Wang,[1,3] Chulu Huang,[1,3] Yunpeng Wu,[1,3] Panpan Yu,[1] Ziqi Chen,[1] Xinxin Li,[1] Hongxia Du,[1] Zhenjiang Zhao,[1] Huan He,[1,2,*] Lili Zhu,[1,*] and Honglin Li[1,2,*]

*Correspondence: hhe@pharm.ecnu.edu.cn (H.H.); zhulfl@ecust.edu.cn (L.Z.); hlli@ecust.edu.cn (H.L.)

Received: April 2, 2026; Accepted: July 3, 2026; Published Online: July 13, 2026; https://doi.org/10.59717/j.xinn-drugdisc.2026.100029

GRAPHICAL ABSTRACT

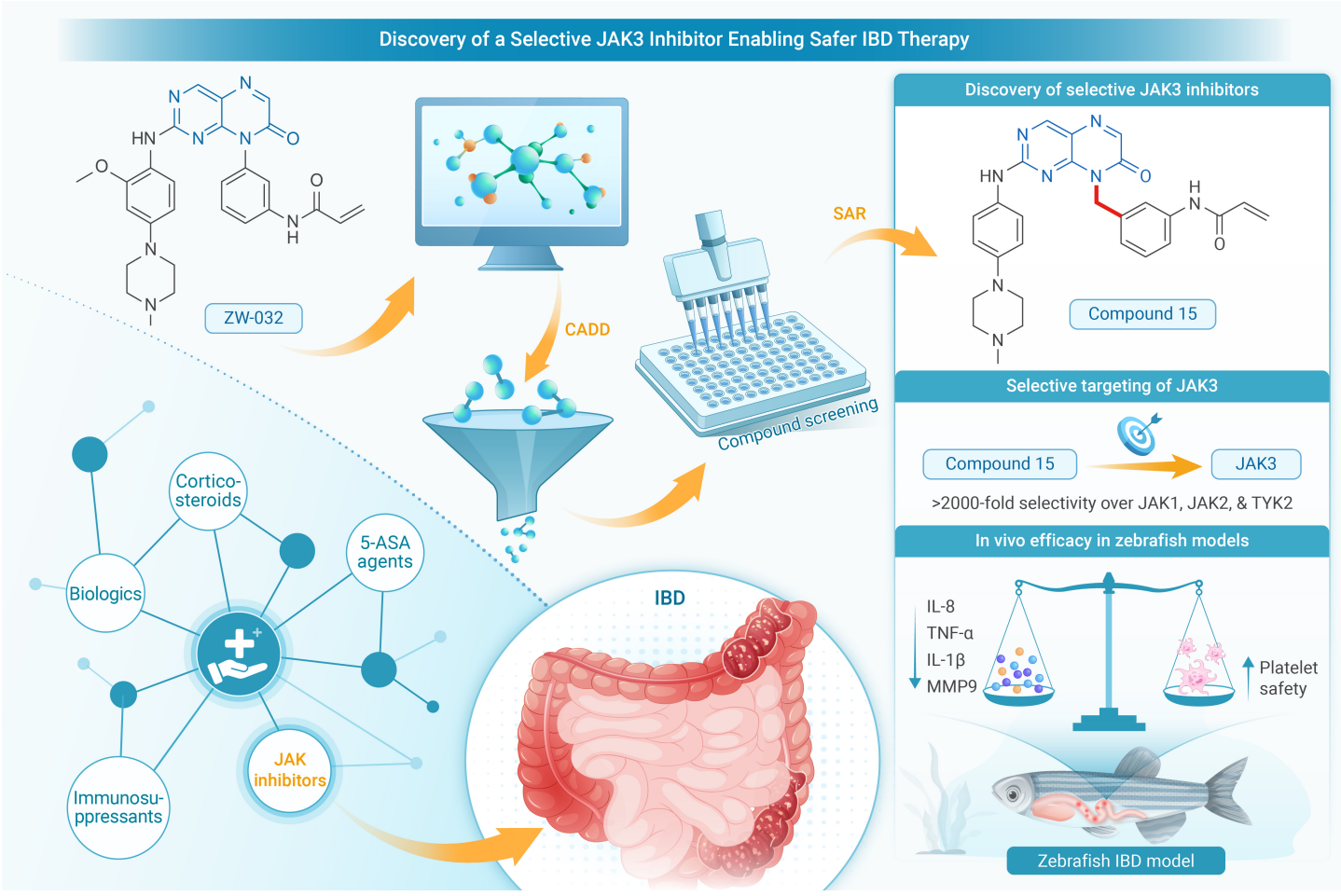

PUBLIC SUMMARY

- We developed Compound 15 as a novel covalent JAK3 inhibitor with excellent subtype selectivity.
- Compound 15 alleviates intestinal inflammation in zebrafish models without thrombocyte depletion.
- This low-toxicity compound serves as a promising IBD therapeutic candidate.

ARTICLE Chemical Biology

OPEN ACCESS

Discovery of a highly selective JAK3 inhibitor for the treatment of inflammatory bowel disease

Caolin Wang,[1,3] Chulu Huang,[1,3] Yunpeng Wu,[1,3] Panpan Yu,[1] Ziqi Chen,[1] Xinxin Li,[1] Hongxia Du,[1] Zhenjiang Zhao,[1] Huan He,[1,2,*] Lili Zhu,[1,*] and Honglin Li[1,2,*]

[1]School of Pharmacy, East China University of Science and Technology, Shanghai 200237, China

[2]Innovation Center for AI and Drug Discovery, School of Pharmacy, East China Normal University, Shanghai 200062, China

[3]These authors contributed equally

*Correspondence: hhe@pharm.ecnu.edu.cn (H.H.); zhulfl@ecust.edu.cn (L.Z.); hlli@ecust.edu.cn (H.L.)

Received: April 2, 2026; Accepted: July 3, 2026; Published Online: July 13, 2026; https://doi.org/10.59717/j.xinn-drugdisc.2026.100029

Citation: Wang C., Huang C., Wu Y., et al. (2026). Discovery of a highly selective JAK3 inhibitor for the treatment of inflammatory bowel disease. *The Innovation Drug Discovery* **1**:100029.

Janus kinase 3 (JAK3) is a promising target for inflammatory bowel disease (IBD). However, the clinical utility of currently approved pan-JAK inhibitors is severely limited by off-target JAK2 inhibition, which is associated with serious side effects such as thrombocytopenia and thrombosis. Herein, a series of pteridine-7(8H)-one derivatives were designed as selective covalent JAK3 inhibitors. Among them, compound 15 exhibited exceptional inhibitory activity against JAK3 (IC_{50} = 0.49 ± 0.05 nM) and a remarkable selectivity profile (> 2000-fold over JAK1, JAK2 and TYK2). Notably, compound 15 significantly attenuated intestinal inflammation in a zebrafish IBD model. Moreover, it showed no risk of inducing thrombocytopenia even at high doses, contrasting with the adverse effects observed with tofacitinib. Its superior selectivity profile effectively avoids JAK2-mediated off-target effects, positioning compound 15 as a highly promising, low-toxicity covalent inhibitor for the treatment of IBD.

INTRODUCTION

The JAK (Janus kinase) family is a class of receptor-associated non-receptor tyrosine kinases consisting of four members: JAK1, JAK2, JAK3, and TYK2. The JAK kinase family mediates intracellular and extracellular signal transduction through the JAK-STAT signaling pathway, which is widely involved in physiological and pathological processes such as immune regulation, cell proliferation, differentiation, and inflammatory responses.[1-2] The JAK-STAT signaling cascade is initiated upon the specific binding of cytokines to their respective receptors, which induces receptor dimerization and subsequent JAK activation. Activated JAKs further phosphorylate tyrosine residues in the intracellular domain of the receptor, forming phosphorylation sites for STAT proteins. Once phosphorylated by JAKs, STAT proteins dimerize, translocate to the nucleus, and directly bind to the DNA promoter region to regulate target gene transcription.[3] The JAK-STAT signaling pathway is widely involved in the signal transduction of multiple cytokines, with different JAKs corresponding to different cytokine receptors.[4] For example, JAK3 primarily couples with common gamma chain (γc) receptors, which are indispensable for lymphocyte development.[5] Unlike the widespread distribution of the other three kinases in the body, JAK3 is exclusively expressed in hematopoietic and immune system cells.[6-7] JAK2 binds to hormone-like cytokines (such as erythropoietin (EPO), thrombopoietin (TPO)) and receptors for IL-3 and GM-CSF, playing a dominant role in hematopoiesis.[8] TYK2 and JAK1 are broadly involved in transmitting inflammatory signals related to interferons (IFN), IL-6, and IL-12/IL-23. Given the distinct tissue distribution and biological functions of each JAK isoform, the development of isoform-selective JAK inhibitors to avoid off-target toxicities has become the core direction of next-generation anti-inflammatory drug development, replacing the non-selective pan-JAK inhibition strategy.

Inflammatory bowel disease (IBD), mainly encompassing ulcerative colitis (UC) and Crohn's disease (CD), is a group of chronic and relapsing gastrointestinal inflammatory disorders.[9] Currently, a diverse range of treatment modalities are available for IBD, including 5-aminosalicylates, corticosteroids, immunosuppressants, and biological agents such as anti-TNF-α antibodies.[10-12] Regrettably, approximately 30%-40% of patients respond poorly to these traditional therapies, and even for those who initially show efficacy, the treatment effect may decline over time.[10] Moreover, long-term use of these drugs often leads to a series of serious side effects, such as a significant increase in susceptibility to infections, an elevated risk of osteoporosis, and varying degrees of damage to liver and kidney functions.[13-15] The JAK-STAT signaling pathway regulates immune cell differentiation, inflammatory responses, and intestinal epithelial homeostasis by mediating cytokine receptor signal transduction.[16-17] During the pathogenesis of IBD, the overactivation of the JAK3 signaling pathway leads to the abnormal activation and proliferation of T lymphocytes, especially Th1, Th2, and Th17 cells.[18] These cells, as the main sources of pro-inflammatory cytokines, secrete a large number of related factors, further exacerbating intestinal inflammation. For instance, IL-21, through the JAK3-STAT pathway, can significantly enhance the ability of T cells to produce IFN-γ and IL-17, thereby further promoting the development of intestinal inflammation.[17] Therefore, targeting JAK3 to treat IBD is a potential therapeutic strategy.

Among the currently approved JAK inhibitors, most are non-selective JAK inhibitors (Figure 1). For example, tofacitinib (**1**), which inhibits JAK1/2/3, was approved by the FDA for UC.[19-20] However, its broad-spectrum inhibition leads to dose-limiting toxicities directly derived from off-target JAK2 blockade. As JAK2 is indispensable for EPO/TPO-mediated erythropoiesis and myelopoiesis, non-specific JAK2 inhibition disrupts normal hematopoietic function, resulting in high incidences of anemia, leukopenia, and thrombocytopenia in clinical practice.[21] Meanwhile, non-selective inhibition of JAK1, which is involved in multiple homeostatic immune and anti-inflammatory pathways, further increases the risk of severe opportunistic infections, thromboembolic events, and cardiovascular adverse events (MACE).[22] These risks prompted the FDA to issue a black box warning and restrict its use in high-risk populations.

In this context, the development of isoform-specific JAK3 inhibitors has emerged as the most rational next-generation direction for IBD treatment, owing to the unique restricted expression of JAK3 in immune cells and its non-essential role in systemic hematopoiesis. To address these limitations, selective JAK3 inhibitors have become a research focus. Due to the high homology of the JAK kinase family on the kinase domain JH1, the development of selective JAK3 inhibitors is facing challenges. Ritlecitinib (5) is currently the only approved selective JAK3/TEC inhibitor for alopecia areata and is undergoing Phase III clinical trials for moderate-to-severe UC.[23] It achieves highly selective inhibition of JAK3 by covalently binding to the unique Cys909 residue of JAK3.[24] This agent specifically blocks JAK3-STAT signaling driven by γc cytokines, thereby suppressing Th1/Th17 cell differentiation and pro-inflammatory cytokine release. Importantly, it preserves JAK1-mediated anti-inflammatory pathways (e.g., IL-10, IL-27),[25] avoiding the risk of weakened anti-inflammatory responses caused by pan-JAK inhibitors that indiscriminately inhibit JAK1. In a randomized, double-blind, placebo-controlled Phase IIb clinical study, both oral ritlecitinib and the TYK2/JAK1 inhibitor brepocitinib demonstrated significant efficacy in treating moderate-to-severe active UC. Furthermore, the ritlecitinib group exhibited a lower incidence of infections (8.7%) compared to brepocitinib (16.9%), highlighting its potential for a more favorable efficacy-safety balance.[26] Multiple preclinical selective JAK3 inhibitors including FM-381 (6), Z583 (7) and 12n (8) exhibit excellent kinase activity and isoform selectivity, further enriching the chemical space of this class of inhibitors and providing more options for subsequent drug development.[27-29] Notably, the research and development enthusi-

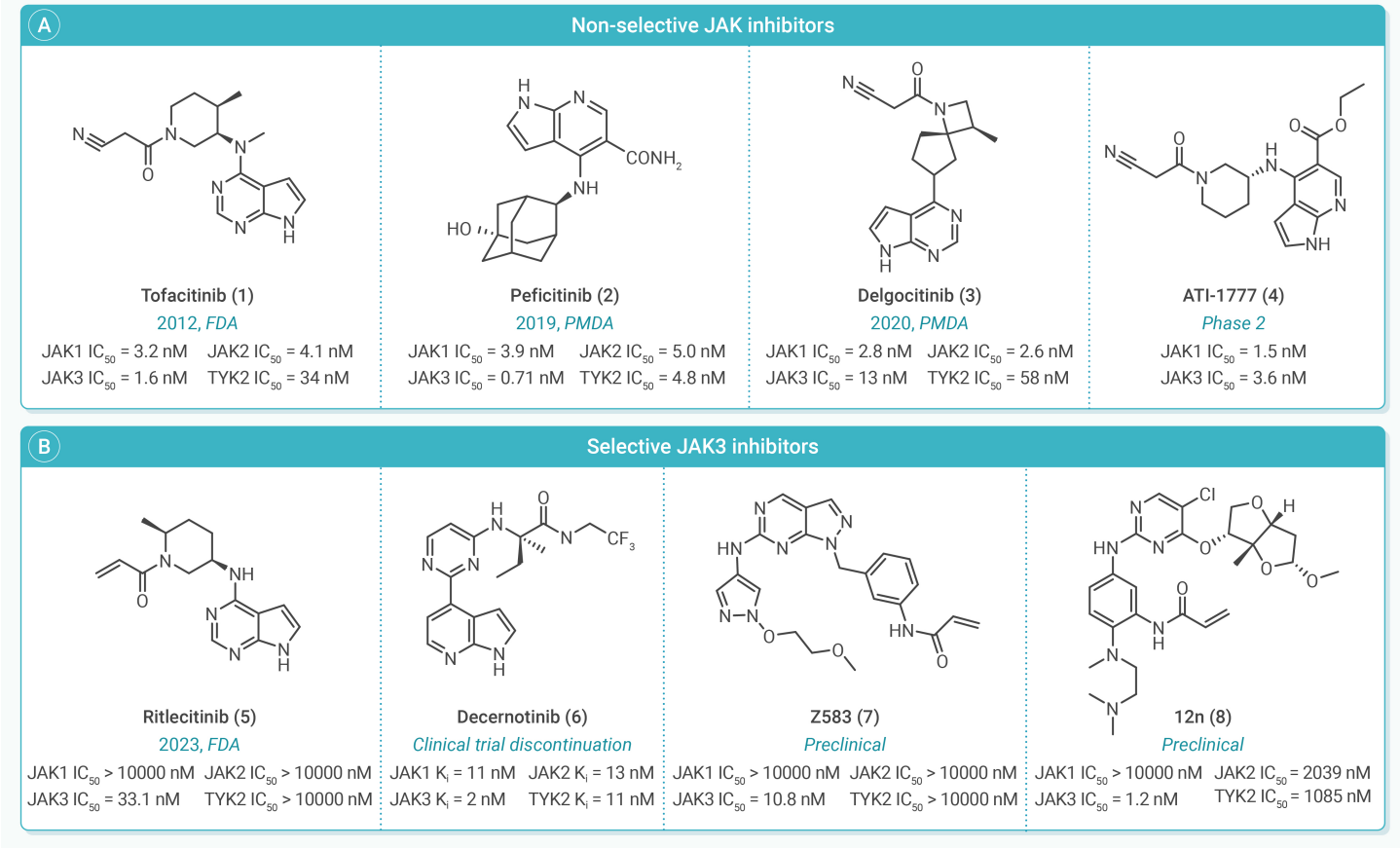

Figure 1. The structures and activities of (A) non-selective JAK inhibitors and (B) selective JAK3 inhibitors

asm for highly selective JAK3 inhibitors continues unabated, with several key studies emerging recently, demonstrating broad application prospects in different therapeutic areas.[30-32]

Building upon these insights, systematic screening of our compound library was performed, leading to the identification of ZW-032 as a promising JAK3 lead inhibitor, with an IC_{50} of 113.83 ± 23.48 nM (Figure 2). Subsequent structure-based optimization yielded compound 15, a highly selective JAK3 inhibitor exhibiting remarkable potency (IC_{50} = 0.49 ± 0.05 nM). Notably, compound 15 possesses a unique pteridinone-7(8H)-one core, which represents a novel chemical scaffold for selective covalent JAK3 inhibitors that is distinct from ritlecitinib and other reported acrylamide-based agents. *In vivo* evaluation in a zebrafish model of IBD further highlighted its therapeutic potential. In transgenic (CD41: eGFP) zebrafish, compound 15 demonstrated a lower risk of inducing thrombocytopenia compared to tofacitinib. These findings highlight compound 15 as a promising candidate for developing selective JAK3-targeted therapies against IBD.

RESULTS

Chemistry

The synthesis of compounds 6-23 is outlined in Scheme 1. The synthetic route initiates with substrate 1a, which undergoes two consecutive aromatic nucleophilic substitution reactions to afford intermediate 3a. Subsequent iron-mediated reduction of the nitro group in 3a yielded the corresponding aniline intermediate 4a. This amino intermediate then underwent a two-step cyclization process to generate intermediate 5a. The Boc (*tert*-butoxycarbonyl) protecting group was removed using hydrochloric acid in 1,4-dioxane, followed by an acryloylation reaction with acryloyl chloride under potassium carbonate conditions to furnish the final target compound. The Boc (tert-butoxycarbonyl) protecting group was removed with HCl in 1,4-dioxane to give compound 6a. Subsequently, acryloylation of 6a with acryloyl chloride in the presence of potassium carbonate afforded the final target compound.

The synthesis of compounds 24-28 is outlined in Scheme 2, while the preparation of intermediates 19-6a from starting material 2a is depicted in Scheme 1. In the final step, intermediates 19-6a undergo either acryloylation with the corresponding acryloyl chloride via an amide-forming reaction, or amide condensation with the appropriate carboxylic acid to afford the respective target compounds.

The synthesis of compounds 29-31 is outlined in Scheme 3. The synthetic route begins with starting material 1b, which undergoes BH_3-THF complex mediated reduction to afford the corresponding aminomethyl intermediate 2b-c**,** Intermediate 2 b-c, in combination with 4-(4-methylpiperazino) aniline, undergoes stepwise aromatic nucleophilic substitution reactions with starting material 1a to generate intermediate 3 b-c. This intermediate is then subjected to acryloylation with acryloyl chloride, forming intermediate 4b-c. Subsequent iron-mediated reduction of the nitro group in 4b affords intermediate 5b-c. Finally, intermolecular cyclization with ethyl glyoxylate delivers the target compound.

Rational design and discovery of a potent JAK3 inhibitor

To identify high-affinity JAK3 inhibitors, an *in vitro* kinase assay was conducted against our in-house compound library. Compound ZW-032 was found to effectively inhibit JAK3 kinase activity with an IC_{50} of 113.83 ± 23.48 nM. To further optimize the JAK3 inhibitory potency of ZW-032, we performed docking studies and analyzed the binding mode of ZW-032 withinthe JAK3 stucture (PDB: 4Z16)[33], followed by comparative analysis with the binding mode of the original co-crystallized ligand (selective JAK3 inhibitor L9). As shown in Figure 2A-B, both the acrylamide group in ZW-032 and L9 demonstrate a common capacity to form covalent interactions with Cys909 in the JAK3 binding pocket. Notably, ZW-032 fails to form the characteristic hydrogen bond with Asp912 that is observed with ligand L9. Additionally, ZW-032 fails to engage the dual hydrogen bond interactions with Leu905, which may contribute to its suboptimal activity.

Structural analysis revealed that the distance between the amino atom at the 6-position of the pyrimidine ring and the amino atom of the Michael

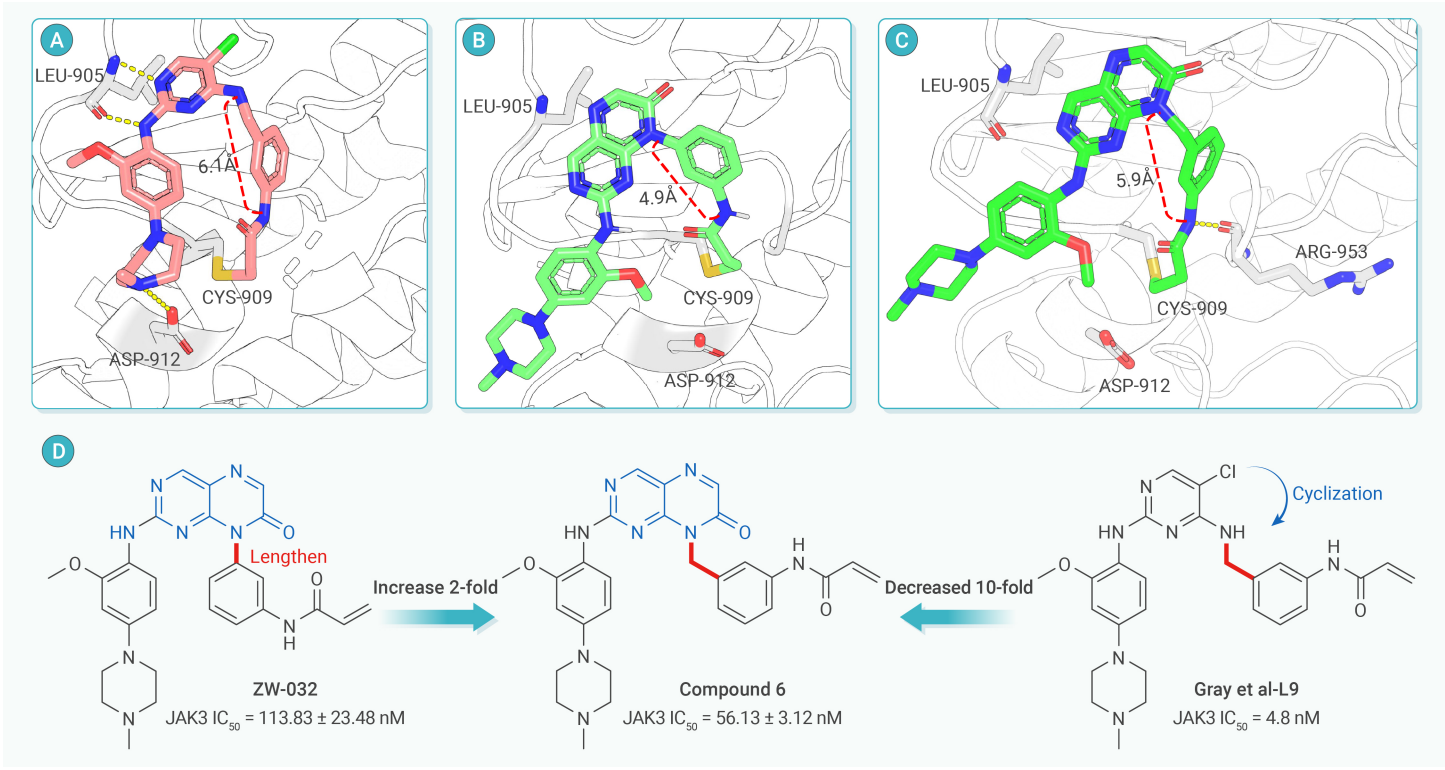

Figure 2. Structure-based optimization of ZW-032 for enhanced JAK3 inhibitory potency (A) Crystal structure of the JAK3 kinase domain in complex with covalently bound L9 (PDB Code: 4Z16)[33]. (B) The docking model of ZW-032 into the JAK3 kinase domain (PDB Code: 4Z16). (C) The docking model of compound 6 into the JAK3 kinase domain (PDB Code: 4Z16). (D) Structural modification of ZW-032 yielded compound 6 with enhanced activity. The hydrogen bond interactions are represented by yellow dashed lines.

acceptor in compound L9 is 6.1 Å (Figure 2A), whereas the corresponding distance in ZW-032 is only 4.9 Å (Figure 2B). This difference likely contributed to ZW-032's failure to approach Leu905. Therefore, inspired by the L9 structure modified by Li Tan et al[33], we introduced a methylene linker between the pteridinone scaffold and the benzene ring of ZW-032, resulting in compound 6 (with the distance adjusted to 5.9 Å). Although the docking model of compound 6 still did not show the anticipated hydrogen bond interaction with Leu905, a new hydrogen bond was observed between the amino group of its acrylamide moiety and Arg953 (Figure 2C). The formation of this newly identified interaction likely accounts for the 2-fold improvement in JAK3 inhibitory potency, with the IC_{50} value decreasing from 113.83 ± 23.48 nM to 56.13 ± 3.12 nM (Figure 2D).

Structural optimization and structure-activity relationship study of novel JAK3 inhibitors

In order to further improve the JAK3 inhibitory activity of compound 6, we analyzed the structure-activity relationship of the aniline side chain systematically (Table 1). Comparison of the docking models of compounds L9, ZW-032 and compound 6 showed that the orientation of the methoxy group on the aniline side chain of L9 adopted an orientation inverse to those observed in the latter two compounds. This suggested that the pteridinone core restricted the binding pocket, providing insufficient space for bulky groups. Based on this structural constraint hypothesis, we specifically designed and synthesized compounds 7-10 to verify the effects of side chain size, aromaticity, and ring system type on activity. Biological evaluation showed that compounds 7 (benzo[*d*][1,2,3]triazole) and 8 (pyridine) exhibited better JAK3 inhibitory activity than compound 6, compound 9 (aromatic five-membered heterocycle) had lower activity, and non-aromatic compound 10 was completely inactive, confirming the aromatic ring as an essential structure and ring system type as an activity-influencing factor. Notably, compound 8, modified by removal of the methoxy group and introduction of a meta-position nitrogen atom, exhibited a two-fold increase in potency over compound 6 (IC_{50} decreased from 56.13 ± 3.12 nM to 27.23 ± 2.01 nM). This further validated the synergistic critical role of eliminating methoxy-induced steric hindrance and regulating the aromatic ring's electronic effect in activity optimization.

Building on these initial SAR insights, we focused on "fine modifications of the benzene ring side chain post-demethoxylation". To this end, we designed and synthesized compounds 11–18, all further modified based on the demethoxylated side chain of compound 6. Our goal was to systematically explore how the type, position and electronic effect of side chain substituents regulate activity. Kinase activity assays showed that all demethoxylated derivatives exhibited JAK3 inhibitory activity superior to that of compound 6. Among them, compounds 14, 15, and 17 achieved nanomolar-level activity, with compound 15 showing the most significant improvement (IC_{50} = 0.49 ± 0.05 nM). Further analysis revealed three critical SAR trends. First, comparisons between compounds 11–13 and compound 6 showed that additional substitutions on the piperazine nitrogen reduced JAK3 inhibitory activity, confirming this nitrogen atom as a key site for maintaining high potency. Second, comparisons among compounds 14–16 indicated that replacing the methyl group on the piperazine ring with either ethyl or deuterated methyl groups led to a decrease in activity. Third, the introduction of halogen substituents at the meta-position of the benzene ring, specifically in compound 17 (fluoro-substituted) and compound 18 (chloro-substituted), resulted in lower activity compared to compound 15. Moreover, compound 18 displayed lower activity than compound 17, which aligns with the structural constraints at this site. The limited space in this region makes larger substituents, such as Cl, more susceptible to steric clashes than smaller ones like F.

Given that compound 15 exhibited the most potent JAK3 inhibitory activity, we conducted a systematic structure-activity relationship (SAR) study based on this compound to investigate the feasibility of enhancing its JAK3 inhibitory potency through further structural modifications. Further analysis via molecular docking models revealed that the C-6 position of the pteridinone core points toward an unoccupied hydrophobic subpocket within the protein binding site (Figure S1). Based on this finding, we designed and synthesized compounds 19–23 by introducing various types of substituents at the C-6 position (Table 2), aiming to systematically evaluate the steric tolerance of this site and the regulatory effect of occupying the subpocket via substituents on activity. Biological evaluation results demon-

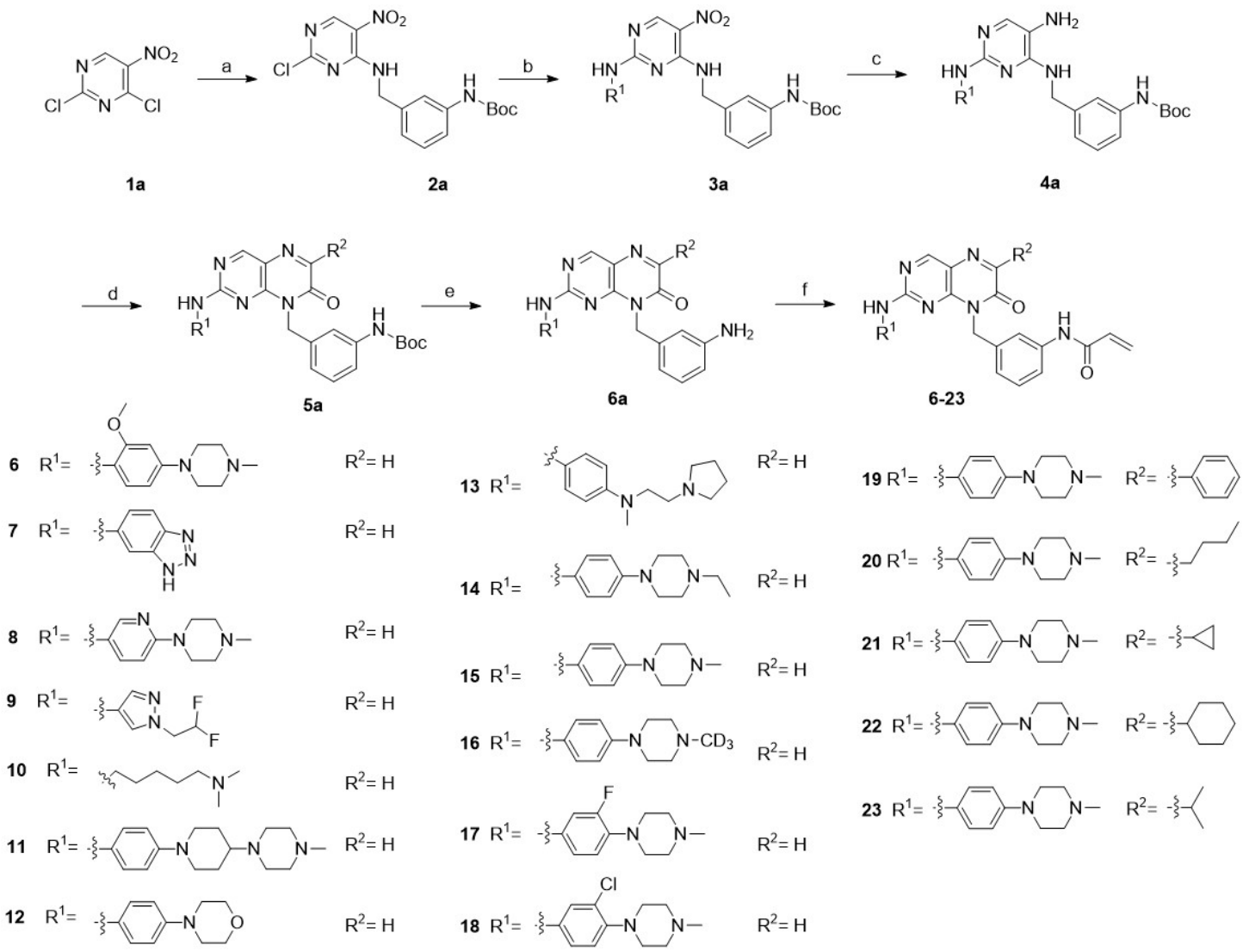

Scheme 1. Synthesis of compounds 6-23[a]. [a]Reagents and conditions (a) *tert*-butyl (3-(aminomethyl)phenyl)carbamate or *tert*-butyl (4-(aminomethyl)pyridin-2-yl)carbamate, DIPEA, MeCN, 0 °C, 1 h, 90%; (b) corresponding amine, DIPEA, THF, RT, 3 h, 65-92%; (c) iron powder, NH_4Cl, EtOH, H_2O, 90 °C, 6 h, 56-88%; (d) corresponding ethyl glyoxylate, EtOH, AcOH, 90 °C, 6 h, 46-59%; (e) trifluoroacetic acid, DCM, RT, 1 h, 84-95%; (f) acryloyl chloride, DCM, 0 °C, 1 h, 58-65%.

strated that all modifications at the C-6 position led to a significant decrease in JAK3 inhibitory activity compared to compound 15. Further analysis showed a prominent volume-dependent negative correlation between substituent size and inhibitory potency. Substituents were ranked by volume: isopropyl (compound 23)> n-butyl (compound 20)> cyclopropyl (compound 21)> cyclohexyl (compound 22). Activity decreased progressively with increasing substituent size, with only the phenyl-substituted analog (compound 19) as an exception. This indicates that any substitution at this position is likely to induce unfavorable steric clashes with amino acid residues in the hydrophobic pocket, ultimately disrupting the critical ligand-protein interactions.

To verify the critical role of covalent warhead binding, we designed and synthesized compounds 24–28, which lack the covalent warhead. Kinase inhibition assays revealed that, compared to compound 15, all derivatives in this series exhibited no detectable JAK3 inhibitory activity (IC_{50} > 1000 nM), with IC_{50} values exceeding 1000 nM (Table 3). These results confirm that covalent binding is essential for JAK3 inhibition and further underscore the pivotal role of the acrylamide pharmacophore.

To further enhance the structure-activity relationship (SAR) profile, we designed and synthesized derivatives 29–31 to systematically evaluate the impact of structural modifications to the acrylamide-linked phenyl ring on JAK3 inhibitory activity. Activity evaluation results demonstrated that modifications at the meta-position of compound 15's phenyl ring significantly regulate its inhibitory potency. Specifically, introducing a fluorine atom (compound 29) caused only a slight activity reduction (IC_{50} = 8.57 ± 0.41 nM). In contrast, introducing the larger chlorine atom (compound 30) led to a marked decrease in potency (IC_{50} = 26.86 ± 1.67 nM). A further comparison of their activities reveals a prominent volume-dependent negative correlation between the size of the meta-substituent and inhibitory potency—the larger the substituent volume, the weaker the inhibitory activity. Additionally, replacing the phenyl ring with a pyridine moiety (compound 31) resulted in substantial activity attenuation.

Molecular docking analysis of compound 15

Subsequent molecular docking studies were performed to clarify the molecular basis for compound 15's potent activity (Figure 3). As an optimized derivative of ZW-032 incorporating the structural merits of L9, compound 15 retained nearly all key binding characteristics of L9 while overcoming the limitations of ZW-032, resulting in a significant enhancement in inhibitory potency. Analysis of the binding mode highlighted several critical optimizations. First, similar to L9, compound 15 formed critical bidentate hydrogen bonds with Leu905 via the pyrimidine nitrogen of the pteridinone core and the amine hydrogen of the side chain—an interaction that was absent in ZW-032. This deficiency in ZW-032 likely stems from an unfavorable distance (4.9 Å) between the scaffold and the Michael acceptor. In contrast, compound 15 optimized this distance to 5.9 Å, aligning with the

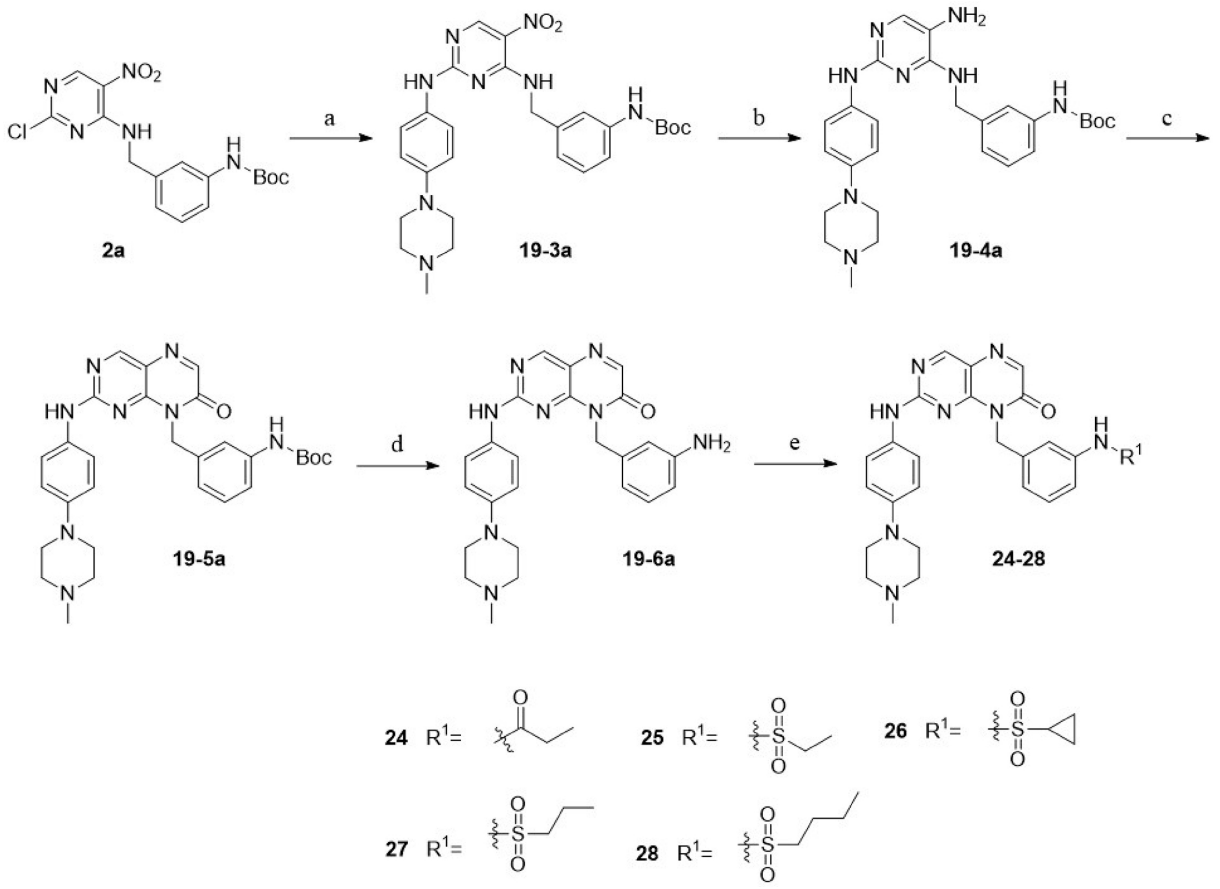

Scheme 2. Synthesis of compounds 24-28[a]. [a]Reagents and conditions (a) 4-(4-methylpiperazino)aniline, DIPEA, THF, RT, 2 h, 81%; (b) iron powder, NH_4Cl, EtOH, H_2O, 90 °C, 6 h, 85%; (c) ethyl glyoxylate, EtOH, AcOH, 90 °C, 2 h, 55%; (d) trifluoroacetic acid, DCM, RT, 1 h, 95%; (e) corresponding acyl chlorides, Cs_2CO_3, DCM, 0 °C or corresponding carboxylic acids, DCC, DCM, 0 °C to RT, 2 h, 59-88%.

spatial arrangement of L9 and enabling stable dual engagement with Leu905. Second, both compound 15 and L9 maintained a stable covalent bond between the acrylamide warhead and Cys909 with a favorable spatial orientation. While ZW-032 also retained this covalent interaction, its warhead orientation was less optimal; in contrast, compound 15 mirrored L9's precise positioning, thereby enhancing binding stability. To determine whether compound 15 functions as a covalent inhibitor, we examined its time-dependent inhibition of JAK3. Compound 15 was evaluated using the Z'-LYTE assay, with pre-incubation times ranging from 0 to 60 min prior to the kinase reaction. Prolonged pre-incubation of compound 15 with JAK3 resulted in a

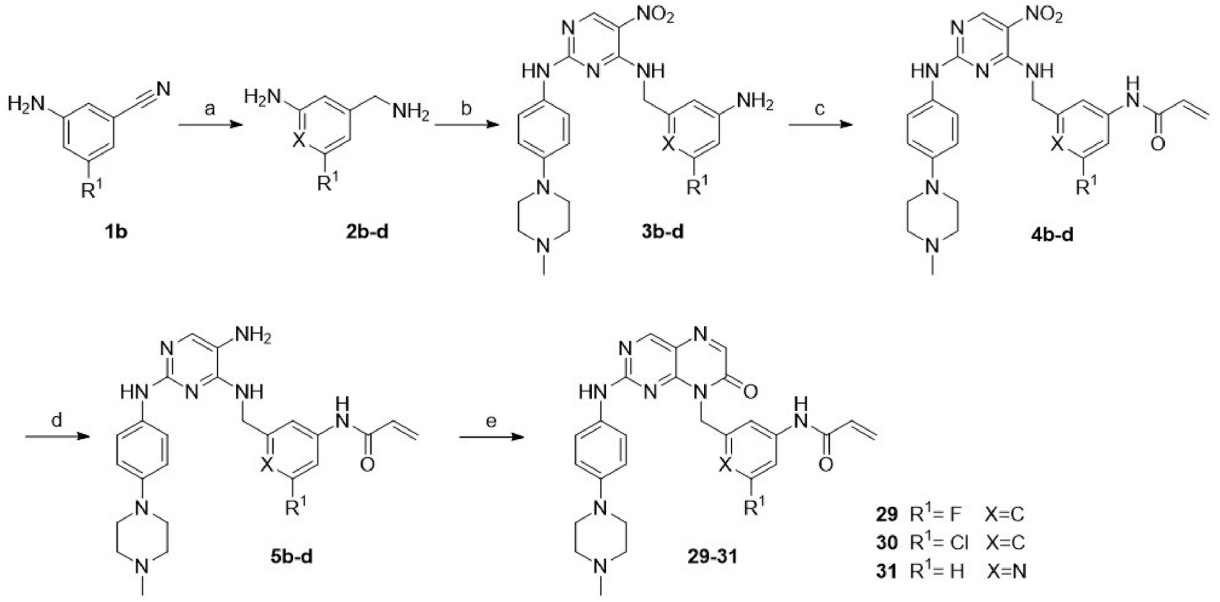

Scheme 3. Synthesis of compounds 29-31[a]. [a]Reagents and conditions (a) BH_3.THF, THF, 70 °C, 1 h, 88-99%; (b) (i) 2,4-dichloro-5-nitropyrimidine, DIPEA, MeCN, 0 °C, 0.5 h, (ii) 4-(4-methylpiperazino)aniline, DIPEA, THF, RT, 2 h, 35-50% (two steps); (c) acryloyl chloride, K_2CO_3, DCM, 0 °C, 3 h, 66-85%; (d) iron powder, NH_4Cl, EtOH, H_2O, 90 °C, 6 h, 55-61%; (e) ethyl glyoxalate, EtOH, AcOH, 90 °C, 6 h, 57-77%.

Table 1. *In vitro* JAK3 kinase inhibitory activities of compounds 6-18.

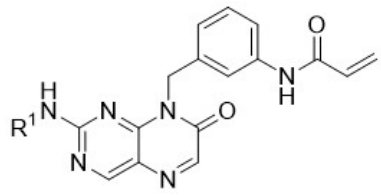

Compd.	R^1	JAK3 (nM)	Compd.	R^1	JAK3 (nM)
6	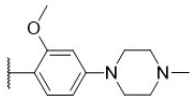	56.13 ± 3.12	13	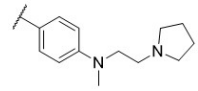	23.75 ± 0.92
7	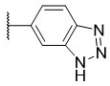	42.82 ± 2.95	14	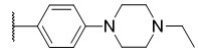	4.62 ± 0.52
8	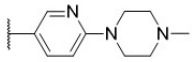	27.23 ± 2.01	15	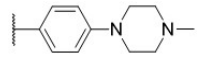	0.49 ± 0.05
9	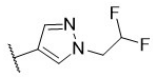	106.35 ± 9.21	16	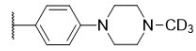	18.21 ± 1.59
10	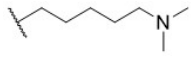	> 1000	17	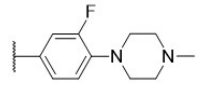	6.21 ± 0.32
11	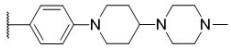	40.31 ± 2.34	18	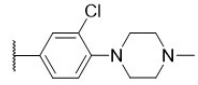	35.38 ± 2.75
12	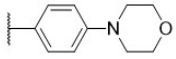	45.21 ± 3.16			

time-dependent increase in inhibition, a trait shared with the covalent inhibitor ritlecitinib. By contrast, the reversible inhibitor tofacitinib exhibited no such time dependency (Figure S2). Third, the piperazine nitrogen in compound 15 formed a hydrogen bond with Asp912, an interaction shared with L9 but lacking in ZW-032. Collectively, these synergistic interactions, characterized by the retention of L9's key features and the rectification of ZW-032's shortcomings, substantially strengthened the ligand-protein binding and directly contributed to the markedly improved JAK3 inhibitory potency of compound 15.

JAK family kinase selectivity analysis of compound 15

Selective JAK3 inhibitors are strategically designed to circumvent the off-target toxicities associated with pan-JAK inhibition. In this study, compound 15 was evaluated for its isoform-selectivity within the JAK kinase family. Compound 15 exhibited exceptional JAK3 selectivity (Table 4), with IC_{50} values> 1000 nM against JAK1, JAK2, and TYK2, significantly surpassing the pan-JAK inhibitor tofacitinib. Notably, it also outperformed the approved selective JAK3 inhibitor ritlecitinib. Ritlecitinib showed JAK family isoform selectivity (IC_{50}> 1000 nM for JAK1/JAK2/TYK2) but had approximately 5-fold lower JAK3 inhibitory potency (IC_{50} = 2.43 ± 0.25 nM) than compound 15. This family selectivity is derived from the unique Cys909 of JAK3, while other kinases have a serine at the same position[34]. Therefore, introducing cysteine-reactive groups, such as acrylamide, into inhibitors can significantly enhance the compound's selectivity within the JAK kinase family.

Kinase spectrum analysis of compound 15

To investigate the selectivity profile of compound 15 at the enzyme level, we profiled compound 15 against a panel of 468 kinases at the concentration of 100 nM (Table S1). Specifically, compound 15 demonstrated exceptionally high binding affinity toward JAK3 kinase, with a % control value of 0.65% (Figure 4, Table S1). Moderate binding activity was also detected for CSF1R (% control value: 1.4) and FLT3 (% control value: 4.7/5.0), although the potency was significantly weaker than that for JAK3. In contrast, the inhibitory activity of compound 15 against DYRK1B (% control value: 7.1) and MUSK (% control value: 8.4) was further reduced (Table S1). This compound shows excellent selectivity for kinases that contain a cysteine residue at the position equivalent to Cys909 in JAK3, including BLK, BTK, EGFR, TEC and other related kinases. Based on the kinome-wide profiling results, we conclude that compound 15 exhibits a remarkable selective inhibition advantage towards JAK3 kinase, indicating its potential for good target specificity and a low risk of off-target effects.

Potent therapeutic efficacy of compound 15 in a zebrafish IBD model

Due to concerns about the poor metabolic stability and low oral bioavailability (F = 5.7%) of compound 15 observed in rat pharmacokinetic studies (Table S2), we reasoned that similar limitations would hinder oral absorption

in zebrafish. Therefore, we adopted immersion administration for the *in vivo* efficacy evaluation in the zebrafish IBD model. In this study, we established a chemically induced IBD model in zebrafish through chronic exposure (3 days) to 0.025% dextran sulfate sodium (DSS). First, we treated the DSS-induced zebrafish IBD model with compound 15 at concentrations of 2.5 μM, 5 μM, and 10 μM. By measuring intestinal reactive oxygen species (ROS) levels in zebrafish, we found that compound 15 demonstrated substantial therapeutic effects at a concentration of 5 μM, with efficacy comparable to that of the positive controls tofacitinib and ritlecitinib at the same concentration (Figure S3). Therefore, the 5 μM concentration was selected for subsequent studies. DSS induction led to a significant recruitment of neutrophils to the intestine of zebrafish compared to the control group. Treatment with 5 μM compound 15 effectively reduced the neutrophil recruitment (Figure 5 A-B). Moreover, treatment with compound 15 successfully attenuated oxidative stress levels in the zebrafish intestine (Figure 5 C-D). Additionally, DSS induction markedly upregulated the expression of pro-inflammatory genes, including IL-1β, IL-8, MMP9, and TNF-α, compared to the control group. Treatment with compound 15 significantly downregulated the expression of these inflammatory genes (Figure 5 E-H). These results indicate that compound 15 exerts a prominent anti-inflammatory effect on IBD symptoms in zebrafish. Histological analysis of zebrafish intestinal tissue sections by H&E staining revealed that DSS induction caused significant intestinal pathological changes in zebrafish, characterized by intestinal lumen dilation and reduced mucosal folds (Figure S4). Treatment with 5 μM compound 15 effectively reduced intestinal diameter and restored mucosal folds. These histopathological observations further confirmed the therapeutic effect of compound 15 against IBD at the histological level.

Reduced thrombocytopenia risk of compound 15 over tofacitinib

Tofacitinib is associated with hematological safety risks in clinical practice, including FDA warnings regarding thrombosis and clinically reported thrombocytopenia.[35-36] These adverse effects are likely associated with the off-target inhibition of JAK2, which mediates essential thrombopoietin signaling.[21] As assessed by STAT3 phosphorylation (Figure S5), compound

Table 2. *In vitro* JAK3 kinase inhibitory activities of compounds 19-23.

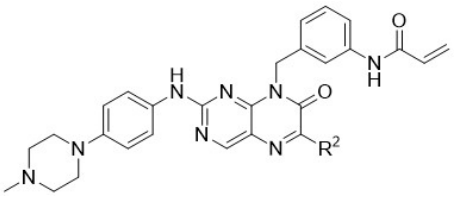

Compd.	R^2	JAK3 (nM)
19		38.54 ± 2.15
20		53.57 ± 4.12
21		154.48 ± 11.84
22		180.49 ± 9.12
23		26.38 ± 2.07

Table 3. *In vitro* JAK3 kinase inhibitory activities of compounds 24-31.

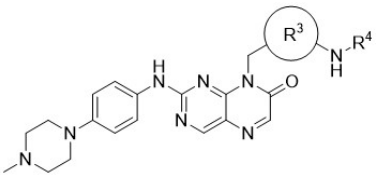

Compd.	R^3	R^4	JAK3 (nM)	Compd.	R^3	R^4	JAK3 (nM)
24	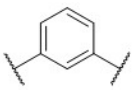		> 1000	28	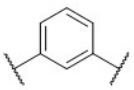	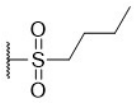	> 1000
25	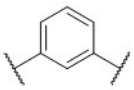		> 1000	29	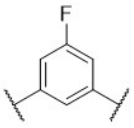	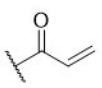	8.57 ± 0.41
26	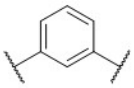		> 1000	30	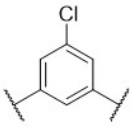	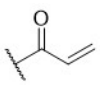	26.86 ± 1.67
27	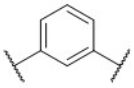	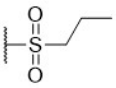	> 1000	31	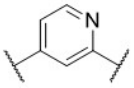	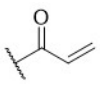	45.85 ± 2.84

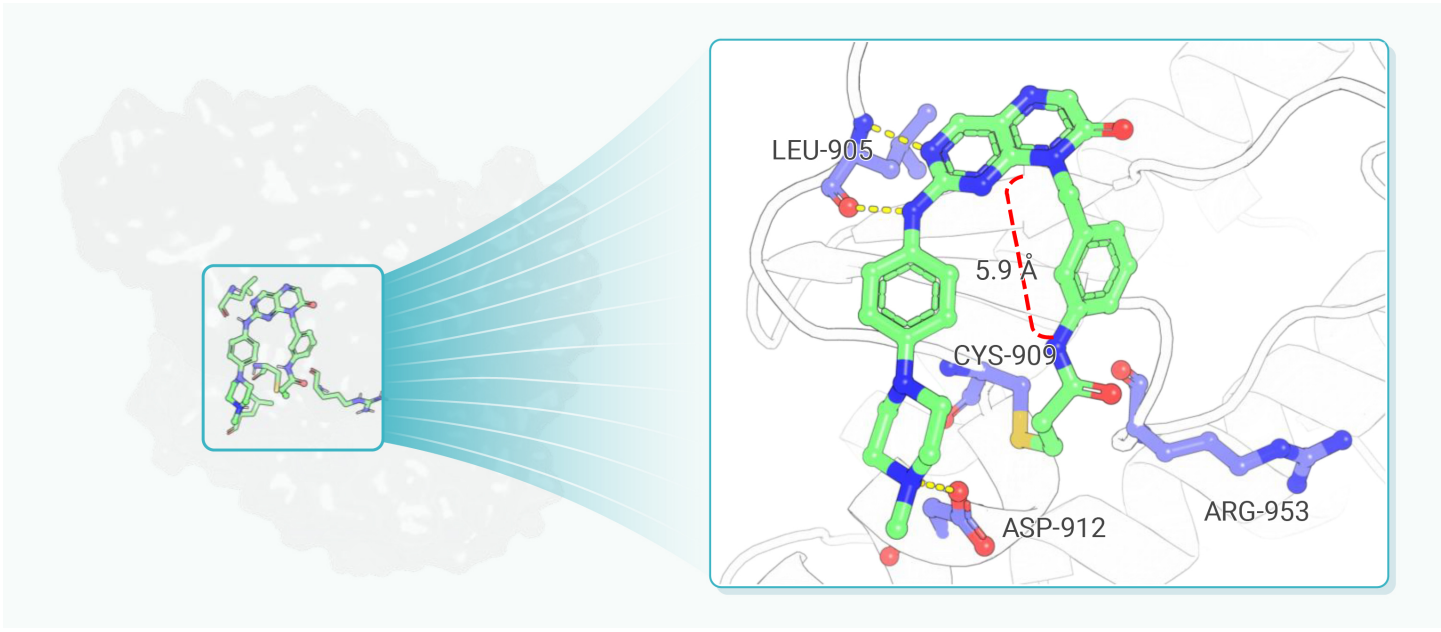

Figure 3. The binding mode of compound 15 into the JAK3 kinase domain. The hydrogen bond interactions are represented by yellow dotted lines

Table 4. JAK family kinase selectivity of compound 15, ritlecitinib and tofacitinib

Compd.	Enzyme inhibitory activity (IC_{50}/nM)			
	JAK1	JAK2	JAK3	TYK2
15	> 1000	> 1000	0.49 ± 0.05	> 1000
Tofacitinib	1.79 ± 0.15	12.43 ± 2.56	1.21 ± 0.11	21.42 ± 1.68
Ritlecitinib	> 1000	> 1000	2.43 ± 0.25	> 1000

15 had no significant effect on the JAK2-dependent signaling pathway, even at doses as high as 10 μM, indicating a lack of observable off-target activity against JAK2-STAT3 signaling. To investigate whether the superior JAK3 selectivity of compound 15 could mitigate these risks, we evaluated its impact on thrombopoiesis using a transgenic zebrafish model Tg (CD41: eGFP). Preliminary toxicity assays demonstrated that concentrations up to 500 μM were well-tolerated by zebrafish embryos, with no significant developmental toxicity observed. At 2 days post-fertilization (2 dpf), embryos were treated with compound 15, tofacitinib (5, 50, and 500 μM) or a vehicle control (0.1% DMSO) for 48 hours. Fluorescent images of platelets were captured via confocal microscopy, and the total fluorescent intensity of platelet spots was quantified using ImageJ. As shown in Figure 6, tofacitinib induced a dose-dependent reduction in platelet fluorescence compared to the control. In contrast, compound 15 exhibited no significant impact on thrombopoiesis across all tested concentrations. These results indicate that the high selectivity of compound 15 for JAK3 effectively mitigates the r isk of thrombocytopenia, offering a safer profile for further clinical development.

CONCLUSIONS

JAK3 has emerged as a high-value therapeutic target for inflammatory bowel disease (IBD), as its restricted expression in hematopoietic and immune cells enables selective inhibition to block pathological inflammation while minimizing systemic off-target toxicities, addressing the core limitations of current IBD treatments. In this study, we identified ZW-032 as a JAK3-active hit compound via library screening, and performed structure-guided rational optimization to develop compound 15, a novel covalent JAK3 inhibitor with excellent potency and isoform selectivity.

Compound 15 exhibited potent JAK3 inhibitory activity with an IC_{50} of 0.49 ± 0.05 nM, and achieved > 2000-fold selectivity over JAK1, JAK2 and TYK2, with no detectable inhibition of other JAK isoforms at 1 μM. Kinome-wide profiling further confirmed its high target specificity and low off-target risk. Structure-activity relationship (SAR) studies revealed that the acrylamide warhead is essential for JAK3 inhibition via covalent binding to the unique Cys909 residue of JAK3, which is also the structural basis for its high isoform selectivity.

Notably, the benzylic methylene linker introduced during structural optimization was considered a potential oxidative metabolic site. However, the measurable systemic exposure and moderate half-life of compound 15 in rats confirmed that this motif does not represent a major metabolic liability, supporting its suitability for further development. In addition, GSH stability data indicated that GSH conjugation is not the primary cause of the rapid clearance (Figure S6), and other mechanisms, such as hepatic metabolism, may play a more dominant role. *In vivo*, compound 15 showed robust anti-inflammatory efficacy in a DSS-induced zebrafish IBD model, as evidenced by reduced intestinal neutrophil infiltration, attenuated oxidative stress, and downregulated expression of pro-inflammatory mediators. Notably, compound 15, unlike the pan-JAK inhibitor tofacitinib, did not adversely affect platelet generation in zebrafish, further supporting its superior safety profile resulting from high JAK3 selectivity. Compared with the clinical selective covalent JAK3 inhibitor ritlecitinib, compound 15 contains a novel pteridinone-7(8H)-one scaffold, shows stronger JAK3 inhibitory activity with equivalent JAK family selectivity, and achieves comparable zebrafish IBD efficacy with a superior safety profile to tofacitinib.

Collectively, compound 15 is a potent, highly selective and low-toxicity JAK3 inhibitor with promising therapeutic potential for IBD. This work not only provides a novel preclinical candidate for IBD treatment, but also offers valuable structural insights for the rational design of selective JAK3 inhibitors for autoimmune diseases.

MATERIALS AND METHODS

All chemicals were obtained from commercial sources (Titan Chemical, Bidepharm, and Energy Chemical) and were used without further purification. The reactions were monitored by thin-layer chromatography (TLC) or LC-MS. The purification of the compounds was done by flash chromatography on

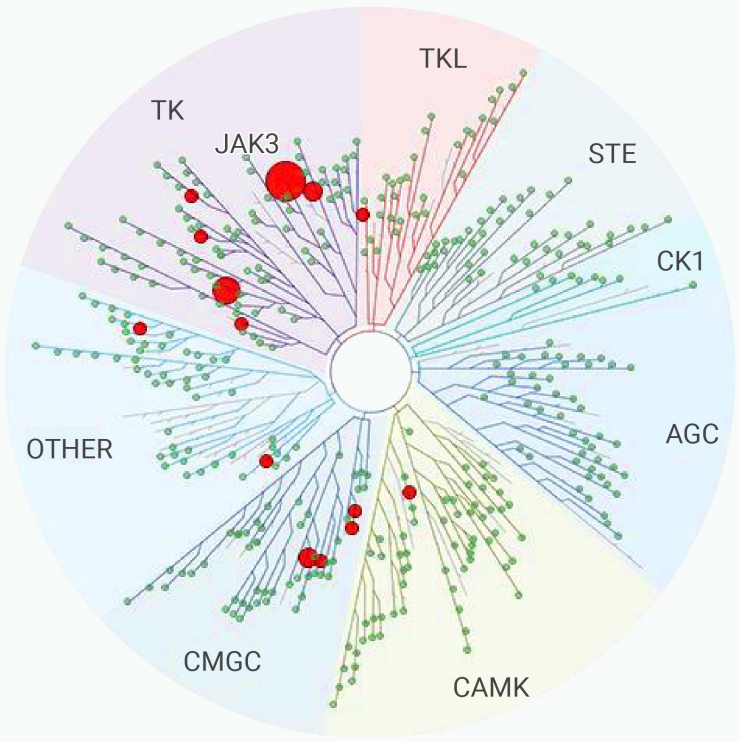

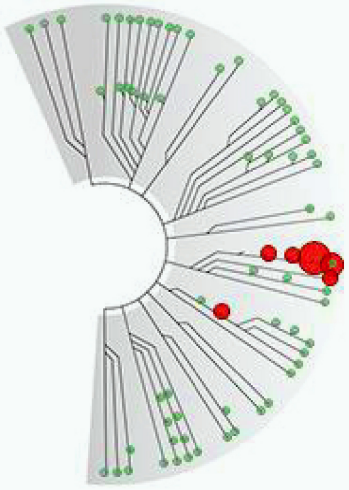

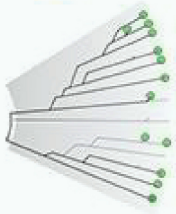

Compound 15
468 assays tested
Selectivity score: 0.002

Percent control

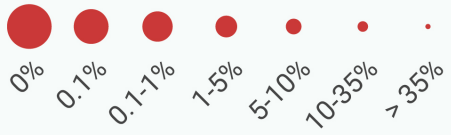

DiscoveRx gene symbol	%Ctrl@100 nM
JAK3 (JH1domain-catalytic)	0.65
CSF1R-autoinhibited	1.4
FLT3 (D835Y)	4.7
FLT3 (D835V)	5
DYRK1B	7.1
MUSK	8.4
CDKL2	10
BLK	13
GCN2 (Kin.Dom.2, S808G)	16
AURKA	19
FLT3(N841I)	20
CSF1R	21
PRKD2	23
FLT3 (K663Q)	24
FLT3 (R834Q)	26
IRAK1	26
CDKL3	28
CLK2	28
BTK	31
KIT (L576P)	33
EPHB6	34

Figure 4. Kinase selectivity profile of compound 15 against 468 kinases

300–400 mesh silica gel (Titan Chemical). All NMR spectra were acquired using an Avance-400 or Ascend 600 spectrometer in DMSO-d_6 or $CDCl_3$ with TMS as an internal standard. Mass spectra for intermediates were recorded on an Agilent 6120 LC-MS device. The microwave reactions were carried out in a microwave reactor (CEM, DISCOVERY). The purity of all target compounds was confirmed to be > 95% by HPLC. HPLC was performed on an Agilent 1200 HPLC device equipped with a 2998 PDA detector taking an Eclipse XDB-C18 reversed-phase column (150 × 4.6 mm, 5 μm). The mobile phase consisted of mobile phase A (CH_3CN) and mobile phase B (0.1% CH_3COONH_4 in water). The flow rate was 0.8 mL/min, with mobile phase A decreasing from 80% to 20% in 3 min and subsequently increasing to 80% within 15 min. The NMR, HRMS, and HPLC data of target compounds are presented in the Supporting Information. All animal experiments involving zebrafish were conducted in accordance with the Guide for the Care and Use of Laboratory Animals of the National Institutes of Health and were approved by the Animal Ethics Committee of East China University of Science and Technology (Permit Number: ECUST-2025-123).

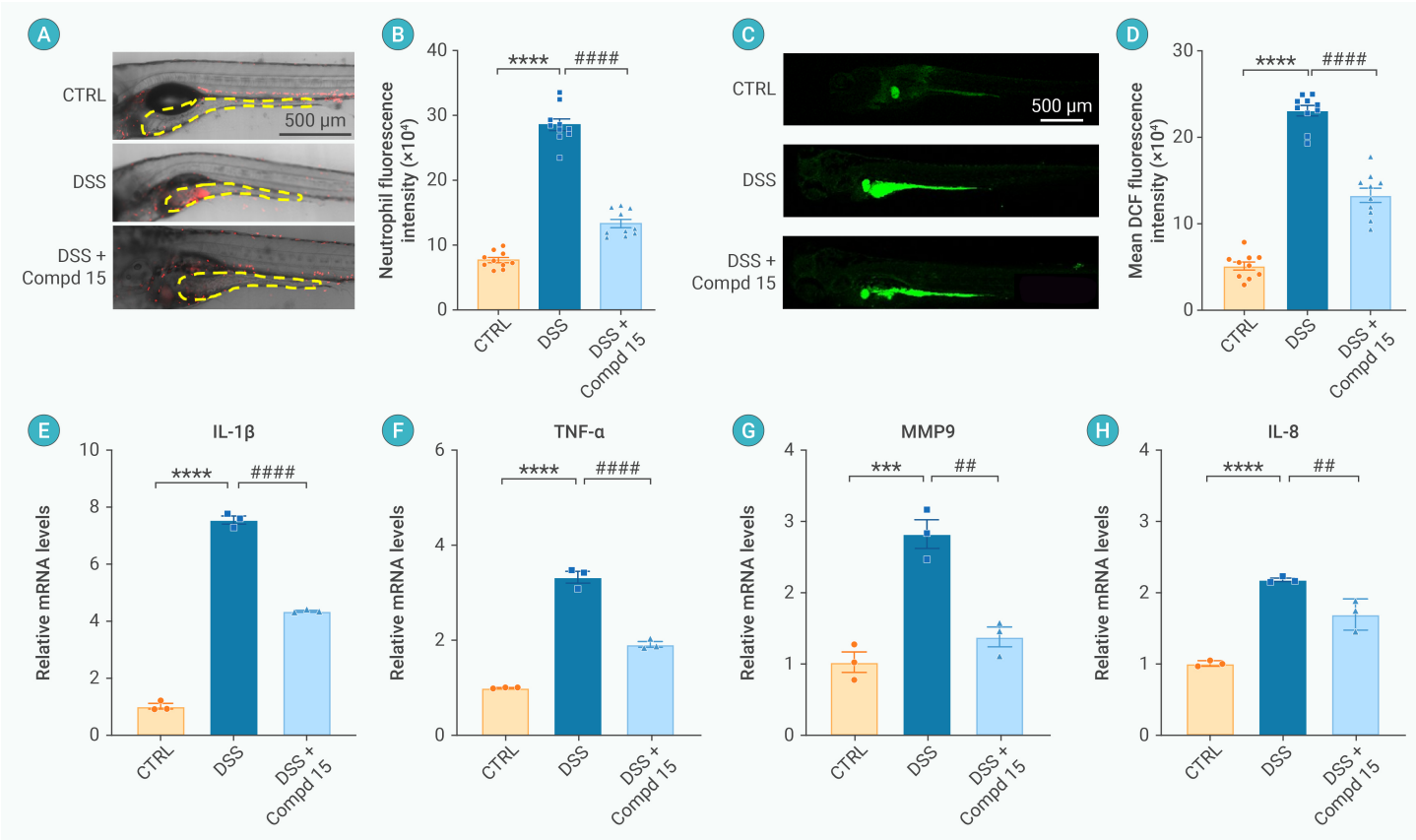

Figure 5. Effects of compound 15 in a zebrafish model of IBD (A) Representative merged fluorescence and bright-field images of the intestinal region in zebrafish from various groups (the intestinal region is outlined by a yellow line); (B) Statistical analysis of neutrophil fluorescence intensity. (C) Representative fluorescence images of the zebrafish intestine stained for ROS; (D) Statistical analysis of DCF fluorescence intensity from (C), $n = 10$. (E-H) Relative mRNA expression levels of pro-inflammatory-related genes, including (E) IL-1β, (F) TNF-α, (G) MMP9, and (H) IL-8. Data are presented as mean ± SEM. Experiments were performed in triplicate wells. *** $P < 0.001$, **** $P < 0.0001$ vs CTRL; ## $P < 0.01$, #### $P < 0.0001$ vs DSS group.

Chemical Synthesis

tert-butyl. (3-(((2-chloro-5-nitropyrimidin-4-yl)amino)methyl)phenyl) carbamate (2a). To a solution of 3-(Boc-amino)benzylamine (5.00 g, 22.51 mmol) and DIPEA (5.82 g, 45.02 mmol) in anhydrous acetonitrile (20 mL) was added to a solution of 2,4-dichloro-5-nitropyrimidine (4.37 g, 22.51 mmol) in anhydrous acetonitrile (10 mL). The reaction mixture was stirred in an ice bath for 0.5 h. Upon completion, the reaction mixture was concentrated under reduced pressure and extracted with water and dichloromethane (DCM) three times (3×70 mL). The combined organic layers were washed with saturated brine, dried over anhydrous sodium sulfate, and concentrated. Purification by silica gel column chromatography (PE/EA = 3:1) to obtain a yellow solid product 2a (7.72 g, 90.4%). ^{1}H NMR (500 MHz, DMSO-d_6, δ): 9.60 (t, J = 6.2 Hz, 1H), 9.27 (s, 1H), 9.06 (s, 1H), 7.43 (s, 1H), 7.34 (d, J = 8.1 Hz, 1H), 7.19 (t, J = 7.9 Hz, 1H), 6.96 (d, J = 7.6 Hz, 1H), 4.69 (d, J = 6.2 Hz, 2H), 1.46 (s, 9H). LC-MS (ESI): m/z: 380.1 $[M+H]^+$.

tert-butyl. (3-(((2-((4-morpholinophenyl)amino)-5-nitropyrimidin-4-yl)amino)methyl)phenyl)carbamate (12-3a). To a solution of 4-morpholinoaniline (140.80 mg, 0.79 mmol) and DIPEA (204.20 mg, 1.58 mmol) in anhydrous tetrahydrofuran (THF, 20 mL), a solution of intermediate 2a (300.00 mg, 0.79 mmol) was added dropwise under stirring. The reaction mixture was stirred at room temperature for 2 hours. Upon completion, the mixture was concentrated under reduced pressure and extracted with DCM (3×15 mL) and water. The combined organic layers were washed with saturated brine, dried over anhydrous sodium sulfate, and concentrated. Purification by silica gel column chromatography (DCM/MeOH = 25/1) afforded the yellow solid product 12-3a (379.50 mg, 92.1%). ^{1}H NMR (500 MHz, DMSO-d_6, δ): 10.19 (s, 1H), 9.37 (t, J = 6.1 Hz, 1H), 9.33 (s, 1H),, 8.97 (s, 1H), 7.45 (s, 1H), 7.36 (t, J = 8.6 Hz, 3H), 7.20 (t, J = 7.8 Hz, 1H), 6.90 (d, J = 7.6 Hz, 1H), 6.77 (d, J = 8.6 Hz, 2H), 4.70 (d, J = 6.1 Hz, 2H), 3.73 (t, J = 4.7 Hz, 4H), 3.04 (t, J = 4.8 Hz, 4H), 1.46 (s, 9H). LC-MS (ESI): m/z: 522.2 $[M+H]^+$.

tert-butyl. (3-(((5-amino-2-((4-morpholinophenyl)amino)pyrimidin-4-yl)amino) methyl)phenyl)carbamate (12-4a). To a solution of intermediate 12-3a (379.50 mg, 0.73 mmol) in ethanol (16 mL) and water (4 mL), iron powder (203.85 mg, 3.65 mmol) and ammonium chloride (NH_4Cl, 390.47 mg, 7.30 mmol) was added. The reaction mixture was stirred at 90 °C for 2 hours. The reaction mixture was hot-filtered through diatomite and concentrated under reduced pressure. The residue was adjusted with saturated sodium bicarbonate solution to pH 9 and extracted with water and ethyl acetate (3×20 mL), the combined organic layers were washed with saturated salt water, dried over anhydrous sodium sulfate and concentrated to obtain a brown solid product 12-4a (316.13 mg, 87.6%). ^{1}H NMR (500 MHz, DMSO-d_6, δ): 9.33 (s, 1H), 8.17 (s, 1H), 7.51 (s, 1H), 7.44 (d, J = 9.0 Hz, 2H), 7.39 (s, 1H), 7.29 (d, J = 8.3 Hz, 1H), 7.18 (t, J = 7.8 Hz, 1H), 6.94 (d, J = 7.6 Hz, 1H), 6.89 (t, J = 5.9 Hz, 1H), 6.73 (d, J = 9.1 Hz, 2H), 4.56 (d, J = 5.8 Hz, 2H), 4.05 (s, 2H), 3.71 (t, J = 4.8 Hz, 4H), 2.95 (t, J = 4.8 Hz, 4H), 1.46 (s, 9H). LC-MS (ESI): m/z: 492.3 $[M+H]^+$.

tert-butyl. (3-((2-((4-morpholinophenyl)amino)-7-oxopteridin-8(7H)-yl)methyl)phenyl)carbamate (12-5a). To a solution of intermediate 12-4a (316.00 mg, 0.64 mmol) in ethanol (15 mL) and acetic acid (1 mL), 50% ethyl glyoxylate toluene solution (263.16 mg, 1.29 mmol) was added. The reaction mixture was stirred at 90 °C for 2 hours. Upon completion, the mixture was concentrated under reduced pressure and adjusted with saturated with saturated sodium bicarbonate solution to pH 9 and extracted with water and ethyl acetate (3×15 mL), the combined organic layers were washed with saturated salt water, dried over anhydrous sodium sulfate and concentrated. Purification by silica gel column chromatography (DCM/MeOH = 25/1) to obtain a brown solid product 12-5a (201.26 mg, 59.4%). ^{1}H NMR (500 MHz, DMSO-d_6, δ): 10.10 (s, 1H), 9.26 (s, 1H), 8.83 (s, 1H), 8.01 (s, 1H), 7.40 (d, J = 9.8 Hz, 3H), 7.31 (s, 1H), 7.18 (t, J = 7.9 Hz, 1H), 6.82 (s, 3H), 5.34 (s, 2H), 3.71 (t, J = 4.8 Hz, 4H), 3.04 (t, J = 4.8 Hz, 4H), 1.44 (s, 9H). LC-MS (ESI): m/z: 530.2 $[M+H]^+$.

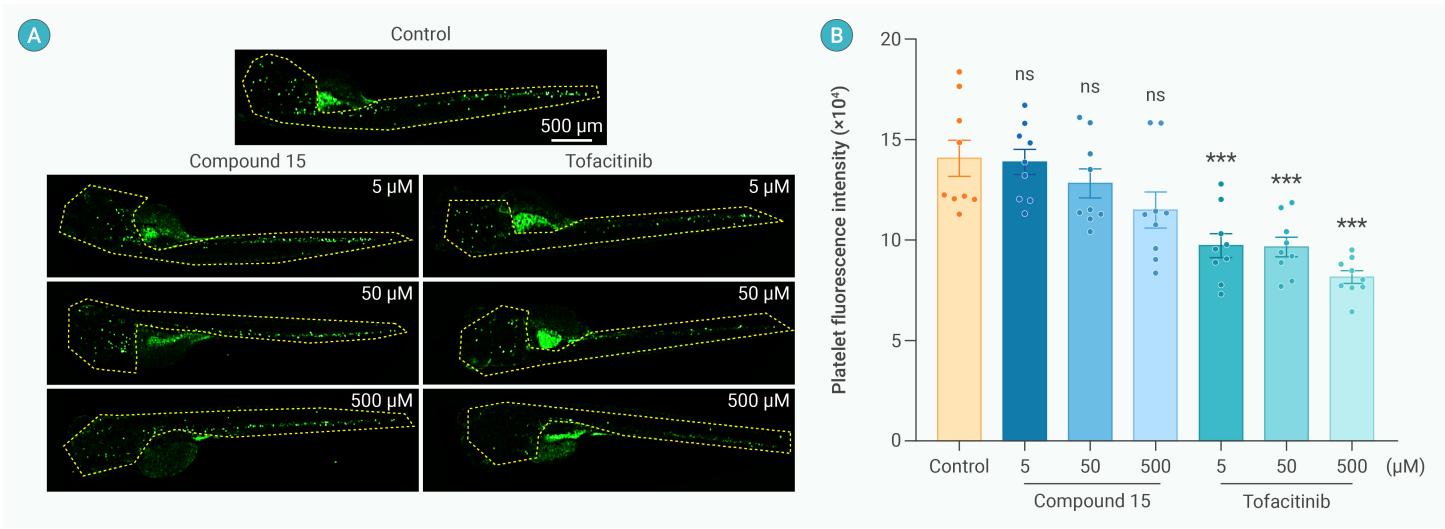

Figure 6. Assessment of compound 15 and tofacitinib on platelet counts in zebrafish (A) Representative fluorescence images of platelets in Tg (CD41: eGFP) zebrafish larvae treated with compound 15 or tofacitinib. (B) Statistical analysis of platelet fluorescence intensity. Data are presented as mean ± SEM, n = 9. *** P < 0.001, **** P < 0.0001 vs control; ns, not significant.

8-(3-aminobenzyl)-2-((4-morpholinophenyl)amino)pteridin-7(8H)-one (12-6a). To a solution of intermediate 12-5a (201.26 mg, 0.38 mmol) in DCM (15 mL), trifluoroacetic acid (5 mL) was added. The reaction mixture was stirred at room temperature. Upon completion, the mixture was concentrated under reduced pressure and adjusted with saturated with saturated sodium bicarbonate solution to pH 9 and extracted with water and DCM (3×20 mL), the combined organic layers were washed with saturated salt water, dried over anhydrous sodium sulfate and concentrated to obtain a brown solid product 16-6a (145.92 mg, 88.2%) without further purification. ^{1}H NMR (500 MHz, DMSO-d_6, δ): 10.09 (s, 1H), 8.82 (s, 1H), 8.00 (s, 1H), 7.47 (d, J = 8.1 Hz, 2H), 6.94 (t, J = 8.1 Hz, 1H), 6.87 (d, J = 8.5 Hz, 2H), 6.42 (d, J = 6.2 Hz, 3H), 5.25 (s, 2H), 5.03 (s, 2H), 3.74 (t, J = 4.8 Hz, 4H), 3.06 (t, J = 4.8 Hz, 4H). LC-MS (ESI): m/z: 430.2 $[M+H]^+$.

N-(3-((2-((4-morpholinophenyl)amino)-7-oxopteridin-8(7H)-yl)methyl)phenyl)acr ylamide (12). To a solution of intermediate 12-6a (145.92 mg, 0.34 mmol) was dissolved in DCM (10 mL), potassium carbonate (K_2CO_3, 93.84 mg, 0.68 mmol) and acryloyl chloride (30.77 mg, 0.34 mmol) was added. The reaction mixture was stirred at 0 °C for 30 min. Upon completion, the mixture was concentrated under reduced pressure and extracted with water and DCM (3×15 mL) three times. The combined organic layers were washed with saturated brine, dried over anhydrous sodium sulfate, and concentrated. Purification by silica gel column chromatography (DCM/MeOH = 20/1) to obtain a yellow solid product 12 (96.64 mg, 58.8%). ^{1}H NMR (500 MHz, DMSO-d_6, δ): 10.17 (s, 1H), 10.12 (s, 1H), 8.83 (s, 1H), 8.04 (s, 1H), 7.70 (s, 1H), 7.56 (s, 1H), 7.41 (s, 2H), 7.25 (t, J = 8.2 Hz, 1H), 6.81 (s, 3H), 6.41 (t, J = 13.1 Hz, 1H), 6.25 (d, J = 16.9 Hz, 1H), 5.76 (d, J = 10.1 Hz, 1H), 5.37 (s, 2H), 3.71 (s, 4H), 3.01 (s, 4H). HRMS (ESI) calculated for $C_{26}H_{25}N_7NaO_3[M+Na]^+$ = 506.1911, found 506.1949. HPLC purity: 95.13%, retention time: 4.237 min.

N-(3-((2-((2-methoxy-4-(4-methylpiperazin-1-yl)phenyl)amino)-7-oxopteridin-8(7H) -yl)methyl)phenyl)acrylamide (6). Compound 6 was synthesized according to the method of compound 12, orange solid with 21.5% yield. ^{1}H NMR (400 MHz, DMSO-d_6, δ): 10.18 (s, 1H), 8.87 (s, 1H), 8.78 (s, 1H), 7.99 (s, 1H), 7.68-7.50 (m, 2H), 7.35 (d, J = 8.7 Hz, 1H), 7.26-7.15 (m, 1H), 6.72 (s, 1H), 6.62 (d, J = 2.6 Hz, 1H), 6.48-6.36 (m, 2H), 6.23 (d, J = 16.9 Hz, 1H), 5.74 (d, J = 10.2 Hz, 1H), 5.25 (s, 2H), 3.75 (s, 3H), 3.18 (s, 4H), 2.60 (s, 4H), 2.33 (s, 3H). HRMS (ESI) calculated for $C_{28}H_{31}N_8O_3[M+H]^+$ = 527.2441, found 527.2520. HPLC purity: 99.57%, retention time: 1.480 min.

N-(3-((2-((1H-benzo[d][1,2,3]triazol-5-yl)amino)-7-oxopteridin-8(7H)-yl)methyl) phenyl)acrylamide (7). Compound 7 was synthesized according to the method of compound 12, yellow solid with 19.8% yield. ^{1}H NMR (500 MHz, DMSO-d_6, δ): 15.48 (s, 1H), 10.53 (s, 1H), 10.11 (s, 1H), 8.96 (s, 1H), 8.36 (s, 1H), 8.10 (s, 1H), 7.83 (d, J = 8.3 Hz, 1H), 7.62 (d, J = 9.3 Hz, 2H), 7.49 (s, 1H), 7.23 (t, J = 7.9 Hz, 1H), 7.15 (d, J = 7.7 Hz, 1H), 6.37 (dd, J = 17.0, 10.2 Hz, 1H), 6.22 (dd, J = 17.0, 2.0 Hz, 1H), 5.71 (dd, J = 10.1, 2.0 Hz, 1H), 5.45 (s, 2H). HRMS (ESI) calculated for $C_{22}H_{17}N_9NaO_2[M+Na]^+$ = 462.1397, found 462.1408. HPLC purity: 96.56%, retention time: 4.467 min.

N-(3-((2-((6-(4-methylpiperazin-1-yl)pyridin-3-yl)amino)-7-oxopteridin-8(7H)-yl)methyl)phenyl)acrylamide (8). Compound 8 was synthesized according to the method of compound 16, orange-red solid with 23.4% yield.^{1}H NMR (500 MHz, DMSO-d_6, δ): 10.15 (s, 2H), 8.84 (s, 1H), 8.34-8.20 (m, 1H), 8.03 (s, 1H), 7.73 (s, 1H), 7.60 (s, 2H), 7.23 (t, J = 7.2 Hz, 1H), 6.86 (s, 1H), 6.71 (s, 1H), 6.41 (dd, J = 17.0, 10.1 Hz, 1H), 6.24 (dd, J = 16.9, 2.1 Hz, 1H), 5.75 (dd, J = 10.1, 2.1 Hz, 1H), 5.34 (s, 2H), 3.40 (s, 4H), 2.43 (t, J = 5.2 Hz, 4H), 2.24 (s, 3H). HRMS (ESI) calculated for $C_{26}H_{27}N_9NaO_2[M+Na]^+$ = 520.2180, found 520.2195. HPLC purity: 99.10%, retention time: 3.889 min.

N-(3-((2-((1-(2,2-difluoroethyl)-1H-pyrazol-4-yl)amino)-7-oxopteridin-8(7H)-yl)me thyl)phenyl)acrylamide (9). Compound 9 was synthesized according to the method of compound 12, yellow solid with 36.8% yield. ^{1}H NMR (400 MHz, DMSO-d_6, δ): 10.35 (s, 1H), 10.07 (s, 1H), 8.85 (s, 1H), 8.04 (t, J = 16.6 Hz, 1H), 7.76 (s, 1H), 7.63 (t, J = 8.8 Hz, 1H), 7.55 (s, 1H), 7.44 (s, 1H), 7.26 (t, J = 7.7 Hz, 1H), 7.05 (d, J = 7.7 Hz, 1H), 6.36 (dd, J = 17.3, 9.5 Hz, 1H), 6.23 (s, 1H), 5.71 (d, J = 10.0 Hz, 1H), 5.45 (s, 2H), 5.36 (s, 1H), 4.49 (t, J = 14.5 Hz, 2H). HRMS (ESI) calculated for $C_{21}H_{19}F_2N_8O_2[M+H]^+$ = 453.1521, found 453.1598. HPLC purity: 98.93%, retention time: 4.992 min.

N-(3-((2-((5-(dimethylamino)pentyl)amino)-7-oxopteridin-8(7H)-yl)methyl)pheny l)acrylamide (10). Compound 10 was synthesized according to the method of compound 16, orange-red solid with 33.5% yield.^{1}H NMR (400 MHz, DMSO-d_6, δ): 10.10 (s, 1H), 8.67 (s, 1H), 8.16 (t, J = 5.9 Hz, 1H), 7.91 (s, 1H), 7.67-7.58 (m, 1H), 7.54 (t, J = 2.0 Hz, 1H), 7.24 (t, J = 7.9 Hz, 1H), 7.05 (d, J = 7.4 Hz, 1H), 6.38 (dd, J = 16.9, 10.1 Hz, 1H), 6.22 (dd, J = 17.0, 2.1 Hz, 1H), 5.72 (dd, J = 10.0, 2.2 Hz, 1H), 5.33 (s, 2H), 3.26 (q, J = 6.7 Hz, 2H), 2.46 (d, J = 7.3 Hz, 2H), 2.05 (s, 6H), 1.41 (m, 2H), 1.31-1.24 (m, 2H), 1.23-1.16 (m, 2H). HRMS (ESI) calculated for $C_{23}H_{30}N_7O_2[M+H]^+$ = 436.2383, found 436.2462. HPLC purity: 95.35%, retention time: 4.188 min.

N-(3-((2-((4-(4-(4-methylpiperazin-1-yl)piperidin-1-yl)phenyl)amino)-7-oxopteridin-8(7H)-yl)methyl)phenyl)acrylamide (11). Compound 11 was synthesized according to the method of compound 12, orange-red solid with 21.6% yield.^{1}H NMR (500 MHz, DMSO-d_6, δ): 10.19 (s, 1H), 10.08 (s, 1H), 8.83 (s, 1H), 8.03 (s, 1H), 7.67 (s, 1H), 7.58 (d, J = 8.1 Hz, 1H), 7.37 (s, 2H), 7.24 (t, J = 7.9 Hz, 1H), 6.80 (m, 3H), 6.42 (dd, J = 17.0, 10.1 Hz, 1H), 6.25 (dd, J = 17.0, 2.1 Hz, 1H), 5.75 (dd, J = 10.2, 2.1 Hz, 1H), 5.37 (s, 2H), 3.60 (d, J = 12.1 Hz, 4H), 2.56 (m, 4H), 2.40 (m, 4H), 2.27 (m, 1H), 2.20 (s, 3H), 1.81 (d, J = 12.2 Hz, 2H), 1.47 (m, 2H). HRMS (ESI) calculated for $C_{32}H_{37}N_9NaO_2[M+Na]^+$ = 602.2962, found 602.2973. HPLC purity: 98.74%, retention time: 3.899 min.

N-(3-((2-((4-(methyl(2-(pyrrolidin-1-yl)ethyl)amino)phenyl)amino)-7-oxopteridin-8(7H)-yl)methyl)phenyl)acrylamide (13). Compound 13 was synthesized according to the method of compound 12, orange-red solid with

23.4% yield.^{1}H NMR (500 MHz, DMSO-d_6, δ): 10.15 (s, 1H), 10.03 (s, 1H), 8.80 (s, 1H), 8.00 (s, 1H), 7.62 (d, *J* = 8.1 Hz, 1H), 7.56 (s, 1H), 7.36 (s, 2H), 7.24 (t, *J* = 8.0 Hz, 1H), 6.92 (s, 1H), 6.69-6.54 (m, 2H), 6.40 (dd, *J* = 17.0, 10.2 Hz, 1H), 6.23 (dd, *J* = 17.0, 2.1 Hz, 1H), 5.73 (dd, *J* = 10.1, 2.1 Hz, 1H), 5.36 (s, 2H), 3.42 (t, *J* = 7.1 Hz, 2H), 2.85 (s, 3H), 2.73-2.53 (m, 6H), 1.76-1.67 (m, 4H). HRMS (ESI) calculated for $C_{29}H_{32}N_8NaO_2$[M+Na]$^+$ = 547.2540, found 547.2547. HPLC purity: 98.03%, retention time: 4.257 min.

***N*-(3-((2-((4-(4-ethylpiperazin-1-yl)phenyl)amino)-7-oxopteridin-8(7H)-yl)methyl) phenyl)acrylamide (14).** Compound 14 was synthesized according to the method of compound 12, orange-red solid with 14.8% yield.^{1}H NMR (500 MHz, DMSO-d_6, δ): 10.19 (s, 1H), 10.10 (s, 1H), 8.83 (s, 1H), 8.04 (s, 1H), 7.69 (s, 1H), 7.58 (d, *J* = 8.3 Hz, 1H), 7.40 (s, 2H), 7.25 (t, *J* = 7.9 Hz, 1H), 6.97-6.74 (m, 3H), 6.43 (dd, *J* = 17.0, 10.1 Hz, 1H), 6.26 (dd, *J* = 17.0, 2.1 Hz, 1H), 5.76 (dd, *J* = 10.0, 2.1 Hz, 1H), 5.38 (s, 2H), 3.06 (t, *J* = 4.9 Hz, 4H), 2.41 (q, *J* = 7.3 Hz, 2H), 1.05 (t, *J* = 7.2 Hz, 3H). HRMS (ESI) calculated for $C_{28}H_{30}N_8NaO_2$[M+Na]$^+$ = 533.2384, found 533.2397. HPLC purity: 96.13%, retention time: 4.049 min.

***N*-(3-((2-((4-(4-methylpiperazin-1-yl)phenyl)amino)-7-oxopteridin-8(7H)-yl)methyl) phenyl)acrylamide (15).** Compound 15 was synthesized according to the method of compound 12, orange solid with 34.2% yield. ^{1}H NMR (600 MHz, DMSO-d_6, δ): 10.17 (s, 1H), 10.10 (s, 1H), 8.83 (s, 1H), 8.03 (s, 1H), 7.70 (s, 1H), 7.59-7.52 (m, 1H), 7.38 (s, 2H), 7.24 (t, *J* = 7.9 Hz, 1H), 6.90-6.72 (m, 3H), 6.41 (dd, *J* = 17.0, 10.1 Hz, 1H), 6.25 (dd, J = 16.9, 2.0 Hz, 1H), 5.76 (d, *J* = 10.2 Hz, 1H), 5.37 (s, 2H), 3.04 (t, *J* = 4.9 Hz, 4H), 2.43 (t, *J* = 5.0 Hz, 4H), 2.22 (s, 3H). HRMS (ESI) calculated for $C_{27}H_{29}N_8O_2$[M+H]$^+$ = 497.2335, found 497.2414. HPLC purity: 96.53%, retention time: 4.373 min.

***N*-(3-((2-((4-(4-(methyl-d3)piperazin-1-yl)phenyl)amino)-7-oxopteridin-8(7H)-yl) methyl)phenyl)acrylamide (16).** Compound 16 was synthesized according to the method of compound 12, yellow solid with 21.4% yield.^{1}H NMR (500 MHz, DMSO-d_6) δ 10.22 (s, 1H), 10.11 (s, 1H), 8.83 (s, 1H), 8.03 (s, 1H), 7.74 – 7.53 (m, 2H), 7.48 – 7.34 (m, 2H), 7.24 (t, *J* = 7.9 Hz, 1H), 6.83 (d, *J* = 8.1 Hz, 3H), 6.43 (dd, *J* = 17.0, 10.1 Hz, 1H), 6.25 (dd, *J* = 17.0, 2.1 Hz, 1H), 5.76 (dd, *J* = 10.0, 2.0 Hz, 1H), 5.37 (s, 2H), 3.12 (s, 4H), 2.66 (s, 4H). HRMS (ESI) calculated for $C_{27}H_{25}D_3N_8NaO_2$[M+Na]$^+$ = 522.2416, found 522.2428. HPLC purity: 97.12%, retention time: 3.916 min.

***N*-(3-((2-((3-fluoro-4-(4-methylpiperazin-1-yl)phenyl)amino)-7-oxopteridin-8(7H)-yl)methyl)phenyl)acrylamide (17).** Compound 17 was synthesized according to the method of compound 12, orange-red solid with 25.8% yield.^{1}H NMR (400 MHz, DMSO-d_6, δ): 10.28 (s, 1H), 10.16 (s, 1H), 8.90 (s, 1H), 8.08 (s, 1H), 7.63-7.56 (m, 2H), 7.46 (s, 1H), 7.34 (d, *J* = 8.8 Hz, 1H), 7.24 (t, *J* = 8.0 Hz, 1H), 6.98-6.90 (m, 2H), 6.40 (dd, *J* = 16.8, 10.0 Hz, 1H), 6.29-6.18 (m, 1H), 5.77-5.70 (m, 1H), 5.39 (s, 2H), 3.00 (s, 4H), 2.67 (s, 4H), 2.37 (s, 3H). HRMS (ESI) calculated for $C_{27}H_{28}FN_8O_2$[M+H]$^+$ = 515.2241, found 515.2321. HPLC purity: 95.15%, retention time: 1.488 min.

***N*-(3-((2-((3-chloro-4-(4-methylpiperazin-1-yl)phenyl)amino)-7-oxopteridin-8(7H)-yl)methyl)phenyl)acrylamide (18).** Compound 18 was synthesized according to the method of compound 12, yellow solid with 21.4% yield.^{1}H NMR (500 MHz, DMSO-d_6, δ): 10.28 (s, 1H), 10.12 (s, 1H), 8.90 (s, 1H), 8.08 (s, 1H), 7.72 (s, 1H), 7.61-7.50 (m, 3H), 7.24 (t, *J* = 7.9 Hz, 1H), 7.10-6.90 (m, 2H), 6.39 (dd, *J* = 17.0, 10.1 Hz, 1H), 6.23 (dd, *J* = 17.0, 2.1 Hz, 1H), 5.73 (dd, *J* = 10.1, 2.0 Hz, 1H), 5.39 (s, 2H), 2.90 (t, *J* = 4.9 Hz, 4H), 2.47 (s, 4H), 2.24 (s, 3H). HRMS (ESI) calculated for $C_{27}H_{27}ClN_8NaO_2$[M+H]$^+$ = 553.1843, found 553.1847. HPLC purity: 95.13%, retention time: 4.237 min.

***N*-(3-((2-((4-(4-methylpiperazin-1-yl)phenyl)amino)-7-oxo-6-phenylpteridin-8(7H)-yl)methyl)phenyl)acrylamide (19).** Compound 19 was synthesized according to the method of compound 12, orange solid with 29.6% yield. ^{1}H NMR (600 MHz, DMSO-d_6, δ): 10.18 (s, 1H), 10.12 (s, 1H), 8.90 (s, 1H), 8.28-8.19 (m, 2H), 7.73 (s, 1H), 7.63-7.54 (m, 1H), 7.50 (t, *J* = 3.3 Hz, 3H), 7.44 (s, 2H), 7.25 (t, *J* = 7.9 Hz, 1H), 6.93 (s, 1H), 6.82 (d, *J* = 8.6 Hz, 2H), 6.41 (dd, *J* = 16.9, 10.1 Hz, 1H), 6.24 (dd, *J* = 15.5 Hz, 1.8 Hz, 1H), 5.75 (d, *J* = 10.8 Hz, 1H), 5.48 (s, 2H), 3.07 (s, 4H), 2.50 (s, 4H), 2.27 (s, 3H). HRMS (ESI) calcd for $C_{33}H_{33}N_8O_2$[M+H]$^+$ = 573.2648; found 573.2725. HPLC purity: 97.78%, retention time: 4.481 min.

***N*-(3-((6-butyl-2-((4-(4-methylpiperazin-1-yl)phenyl)amino)-7-oxopteridin-8(7H)-yl)methyl)phenyl)acrylamide (20).** Compound 20 was synthesized according to the method of compound 12, orange-yellow solid with 54.7% yield. ^{1}H NMR (400 MHz, DMSO-d_6, δ): 10.16 (s, 1H), 9.90 (s, 1H), 8.77 (s, 1H), 7.69 (s, 1H), 7.55 (d, *J* = 8.0 Hz, 1H), 7.40 (d, *J* = 8.4 Hz, 2H), 7.24 (t, *J* = 8.0 Hz, 1H), 6.80 (d, *J* = 8.8 Hz, 3H), 6.42 (dd, *J* = 17.0, 10.0 Hz, 1H), 6.25 (dd, *J* = 17.0, 2.0 Hz, 1H), 5.76 (dd, *J* = 10.0, 2.0 Hz, 1H), 5.40 (s, 2H), 3.04 (t, *J* = 4.8 Hz, 4H), 2.79 (t, *J* = 7.6 Hz, 2H), 2.45 (t, *J* = 5.2 Hz, 4H), 2.23 (s, 3H), 1.69 (p, *J* = 7.2 Hz, 2H), 1.40 (q, *J* = 7.2 Hz, 2H), 0.93 (t, *J* = 7.2 Hz, 3H). HRMS (ESI) calculated for $C_{31}H_{37}N_8O_2$[M+H]$^+$ = 553.2961, found 553.3038. HPLC purity: 96.49%, retention time: 6.015 min.

***N*-(3-((6-cyclopropyl-2-((4-(4-methylpiperazin-1-yl)phenyl)amino)-7-oxopteridin-8(7H)-yl)methyl)phenyl)acrylamide (21).** Compound 21 was synthesized according to the method of compound 12, orange-yellow solid with 23.5% yield. ^{1}H NMR (400 MHz, DMSO-d_6, δ): 10.16 (s, 1H), 9.85 (s, 1H), 8.67 (s, 1H), 7.65 (s, 1H), 7.59 (d, *J* = 8.0 Hz, 1H), 7.40 (d, *J* = 8.4 Hz, 2H), 7.25 (t, *J* = 8.0 Hz, 1H), 6.90 (s, 1H), 6.80 (d, *J* = 8.4 Hz, 2H), 6.42 (dd, *J* = 16.8, 10.0 Hz, 1H), 6.25 (d, *J* = 16.8 Hz, 1H), 5.76 (d, *J* = 10.0 Hz, 1H), 5.42 (s, 2H), 3.04 (t, *J* = 4.7 Hz, 4H), 2.46 (s, 4H), 2.24 (s, 3H), 1.26-1.21 (m, 1H), 1.11-1.01 (m, 4H). HRMS (ESI) calculated for $C_{30}H_{33}N_8O_2$[M+H]$^+$ = 537.2648, found 537.2727. HPLC purity: 98.35%, retention time: 5.780 min.

***N*-(3-((6-cyclohexyl-2-((4-(4-methylpiperazin-1-yl)phenyl)amino)-7-oxopteridin-8(7H)-yl)methyl)phenyl)acrylamide (22).** Compound 22 was synthesized according to the method of compound 12, orange-yellow solid with 27.4% yield. ^{1}H NMR (400 MHz, DMSO-d_6, δ): 10.17 (s, 1H), 9.90 (s, 1H), 8.76 (s, 1H), 7.71 (s, 1H), 7.55 (d, *J* = 8.0 Hz, 1H), 7.41 (s, 2H), 7.23 (t, *J* = 7.9 Hz, 1H), 6.83-6.78 (m, 3H), 6.42 (dd, *J* = 16.9, 10.1 Hz, 1H), 6.25 (d, *J* = 16.4 Hz, 1H), 5.76 (d, *J* = 10.1 Hz, 1H), 5.40 (s, 2H), 3.14 (t, *J* = 11.6 Hz, 1H), 3.04 (s, 4H), 2.44 (s, 4H), 2.23 (s, 3H), 1.90 (d, *J* = 12.4 Hz, 2H), 1.82 (d, *J* = 12.6 Hz, 2H), 1.51-1.42 (m, 2H), 1.41-1.32 (m, 2H), 1.29-1.20 (m, 2H). HRMS (ESI) calculated for $C_{33}H_{37}N_8O_2$[M-H]$^-$ = 577.3118, found 577.3041. HPLC purity: 95.01%, retention time: 6.640 min.

***N*-(3-((6-isopropyl-2-((4-(4-methylpiperazin-1-yl)phenyl)amino)-7-oxopteridin-8 (7H)-yl)methyl)phenyl)acrylamide (23).** Compound 23 was synthesized according to the method of compound 12, yellow solid with 24.2% yield. 1H NMR (400 MHz, DMSO-d_6, δ): 10.18 (s, 1H), 9.90 (s, 1H), 8.78 (s, 1H), 7.72 (s, 1H), 7.55 (d, *J* = 8.0 Hz, 1H), 7.40 (d, *J* = 7.6 Hz, 2H), 7.24 (t, *J* = 8.0 Hz, 1H), 6.80 (d, *J* = 8.8 Hz, 3H), 6.42 (dd, *J* = 16.8, 10.0 Hz, 1H), 6.25 (dd, *J* = 16.8, 2.0 Hz, 1H), 5.76 (dd, *J* = 10.0, 2.0 Hz, 1H), 5.41 (s, 2H), 3.48-3.38 (m, 1H), 3.04 (t, *J* = 4.8 Hz, 4H), 2.44 (t, *J* = 4.8 Hz, 4H), 2.23 (s, 3H), 1.25 (s, 3H), 1.23 (s, 3H). HRMS (ESI) calculated for $C_{30}H_{35}N_8O_2$[M+H]$^+$ = 539.2805, found 539.2885. HPLC purity: 95.28%, retention time: 5.691 min.

***N*-(3-((2-((4-(4-methylpiperazin-1-yl)phenyl)amino)-7-oxopteridin-8(7H)-yl)methyl) phenyl)propionamide (24).** Compound 24 was synthesized according to the method of compound 12, yellow solid with 35.7% yield. ^{1}H NMR (600 MHz, DMSO-d_6, δ): 10.11 (s, 1H), 9.84 (s, 1H), 8.83 (s, 1H), 8.02 (s, 1H), 7.52 (d, *J* = 7.8 Hz, 2H), 7.43-7.37 (m, 2H), 7.21 (t, *J* = 7.8 Hz, 1H), 6.88-6.78 (m, 3H), 5.35 (s, 2H), 3.07 (t, *J* = 4.8 Hz, 4H), 2.45 (t, *J* = 4.8 Hz, 4H), 2.28 (q, *J* = 7.2 Hz, 2H), 2.22 (s, 3H), 1.05 (t, *J* = 7.8 Hz, 3H). HRMS (ESI) calculated for $C_{27}H_{31}N_8O_2$[M+H]$^+$ = 499.2492, found 499.2568. HPLC purity: 97.58%, retention time: 4.408 min.

***N*-(3-((2-((4-(4-methylpiperazin-1-yl)phenyl)amino)-7-oxopteridin-8(7H)-yl)methyl) phenyl)ethanesulfonamide (25).** To a solution of intermediate 25-6a (30.00 mg, 0.07 mmol) in DCM (10 mL) was added caesium carbonate (Cs_2CO_3, 45.50 mg, 0.14 mmol), pyridine (3 mL) and ethanesulfonyl chloride (10.43 mg, 0.08 mmol) under the ice bath, N_2 was replaced three times. The reaction mixture was stirred stirred at 0 °C. Upon completion, concentrate the mixture and purified by silica gel column chromatography (DCM/MeOH = 10/1) to obtain an yellow solid 25 with 21.9% yield. ^{1}H NMR (400 MHz, DMSO-d_6, δ): 10.13 (s, 1H), 9.75 (s, 1H), 8.84 (s, 1H), 8.01 (s, 1H), 7.45-7.35 (m, 2H), 7.25 (t, *J* = 8.0 Hz, 1H), 7.15 (s, 1H), 7.09 (d, *J* = 8.4 Hz, 1H), 6.94 (s, 1H), 6.88-6.79 (m, 2H), 5.36 (s, 2H), 3.08 (t, *J* = 4.8 Hz, 4H), 2.99 (d, *J* = 7.2 Hz, 2H), 2.47 (t, *J* = 4.8 Hz, 4H), 2.23 (s, 3H), 1.08 (t, *J* = 7.2 Hz, 3H). HRMS (ESI) calculated for $C_{26}H_{31}N_8O_3S$[M+H]$^+$ = 535.2162, found 535.2239. HPLC purity: 99.71%, retention time: 4.481 min.

***N*-(3-((2-((4-(4-methylpiperazin-1-yl)phenyl)amino)-7-oxopteridin-8(7H)-yl)methyl) phenyl)cyclopropanesulfonamide (26).** Compound 26 was synthesized according to the method of compound 25, yellow solid with 24.5% yield. ^{1}H NMR (400 MHz, DMSO-d_6, δ): 10.14 (s, 1H), 9.75 (s, 1H), 8.83 (s, 1H), 8.01 (s, 1H), 7.48-7.37 (m, 2H), 7.25 (t, *J* = 8.0 Hz, 1H), 7.18 (s, 1H), 7.11 (d, *J* = 8.0 Hz, 1H), 6.99-6.93 (m, 1H), 6.84 (d, *J* = 8.8 Hz, 2H), 5.36 (s, 2H),

3.10 (t, *J* = 4.8 Hz, 4H), 2.54-2.47 (m, 4H), 2.26 (s, 3H), 1.28-1.14 (m, 1H), 0.85-0.82 (m, 2H), 0.79 (d, *J* = 10.4 Hz, 2H). HRMS (ESI) calculated for $C_{27}H_{31}N_8O_3S[M+H]^+$ = 547.2162, found 547.2241. HPLC purity: 99.15%, retention time: 4.574 min.

N-(3-((2-((4-(4-methylpiperazin-1-yl)phenyl)amino)-7-oxopteridin-8(7H)-yl)methyl) phenyl)propane-1-sulfonamide (27). Compound 27 was synthesized according to the method of compound 25, yellow solid with 26.7% yield.^{1}H NMR (600 MHz, DMSO-d_6, δ): 10.12 (s, 1H), 9.77 (s, 1H), 8.83 (s, 1H), 8.01 (s, 1H), 7.41 (s, 2H), 7.24 (t, *J* = 7.8 Hz, 1H), 7.13 (s, 1H), 7.08 (dd, *J* = 8.4, 2.4 Hz, 1H), 6.96 (s, 1H), 6.85 (d, *J* = 8.5 Hz, 2H), 5.35 (s, 2H), 3.17 (s, 4H), 2.95 (t, *J* = 7.7 Hz, 2H), 2.77-2.60 (m, 4H), 2.38 (s, 3H), 1.56 (q, *J* = 7.6 Hz, 2H), 0.81 (t, *J* = 7.4 Hz, 3H). HRMS (ESI) calculated for $C_{27}H_{33}N_8O_3S[M+H]^+$ = 549.2318, found 549.2495. HPLC purity: 96.83%, retention time: 4.758 min.

N-(3-((2-((4-(4-methylpiperazin-1-yl)phenyl)amino)-7-oxopteridin-8(7H)-yl)methyl) phenyl)butane-1-sulfonamide (28). Compound 28 was synthesized according to the method of compound 25, yellow solid with 16.4% yield. ^{1}H NMR (400 MHz, DMSO-d_6, δ): 10.12 (s, 1H), 9.75 (s, 1H), 8.84 (s, 1H), 8.01 (s, 1H), 7.40 (s, 2H), 7.26 (t, *J* = 7.6 Hz, 1H), 7.15-7.08 (m, 2H), 6.97 (s, 1H), 6.83 (d, *J* = 8.4 Hz, 2H), 5.36 (s, 2H), 3.10 (s, 4H), 2.95 (t, *J* = 8.0 Hz, 2H), 2.49 (s, 4H), 2.27 (s, 3H), 1.56-1.46 (m, 2H), 1.23-1.17 (m, 2H), 0.72 (t, *J* = 7.2 Hz, 3H). HRMS (ESI) calculated for $C_{28}H_{35}N_8O_3S[M+H]^+$ = 563.2475, found 563.2554. HPLC purity: 96.75%, retention time: 5.065 min.

3-(aminomethyl)-5-chloroaniline (30-2b). To a solution of 3-amino-5-chlorobenzonitrile (770.00 mg, 5.05 mmol) in anhydrous THF (20 mL), 1 M borane-tetrahydrofuran (20 mL) complex was added dropwise at room temperature. The reaction mixture was stirred at 70 °C for 2 hours. Upon completion, the mixture was cooled to 0 °C in an ice-water bath, and 1 M aqueous HCl was slowly added dropwise with stirring until gas evolution ceased. The resulting mixture was stirred at 0 °C for an additional 30 min. The solution was concentrated and the residue was adjusted to pH 9-10 with aqueous sodium hydroxide (NaOH, 2-5 M). The mixture was extracted with DCM (3×70 mL). The combined organic layers was washed with saturated brine, dried over anhydrous sodium sulfate and concentrated to get a yellow oil 30-2b (784.05 mg, 96.7%) without further purification. LC-MS(ESI): m/z: 157.1$[M+H]^+$.

N^4-(3-amino-5-chlorobenzyl)-N^2-(4-(4-methylpiperazin-1-yl)phenyl)-5-nitropyri-midine-2,4-diamine (30-3b). To a solution of 2,4-dichloro-5-nitropyrimidine (975.72 mg, 5.03 mmol) in anhydrous acetonitrile (15 mL) was added dropwise a mixture of 30-2b (784.05 mg, 5.03 mmol) and DIPEA (1.30 g, 10.06 mmol) in anhydrous acetonitrile (30 mL), The reaction mixture was stirred for 5 min. Upon completion, a solution of 4-(4-methylpiperazino)aniline (865.3 mg, 4.53 mmol) and DIPEA (1.17 g, 9.06 mmol) in anhydrous THF (15 mL) were added at 25 °C and stirred for 2 hours The reaction was quenched with water and the mixture was extracted with DCM (3×70 mL). The combined organic layers were washed with saturated brine, dried over anhydrous sodium sulfate concentrated and purified by silica gel column chromatography (DCM/MeOH = 15/1) to obtain a brick-red solid product 30-3b (1.06 g, 50.4%). ^{1}H NMR (500 MHz, DMSO-d_6, δ): 10.22 (s, 1H), 9.36 (t, *J* = 6.2 Hz, 1H), 8.97 (s, 1H), 7.42-7.39 (m, 2H), 6.83 (d, *J* = 8.6 Hz, 2H), 6.49 (s, 1H), 6.45 (d, *J* = 1.8 Hz, 2H), 5.43 (s, 2H), 4.58 (d, *J* = 6.1 Hz, 2H), 3.19 (t, *J* = 5.3 Hz, 4H), 2.69 (s, 4H), 2.39 (s, 3H). LC-MS(ESI): m/z: 469.2$[M+H]^+$.

N-(3-chloro-5-(((2-((4-(4-methylpiperazin-1-yl)phenyl)amino)-5-nitropyrimidin-4-yl)amino)methyl)phenyl)acrylamide (30-4b). To a solution of intermediate 30-3b (124.60 mg, 0.27 mmol) in anhydrous DCM (15 mL) was added K_2CO_3, (73.7 mg, 0.53 mmol). The mixture was cooled to 0 °C in an ice-water bath, and a solution of acryloyl chloride (28.9 mg, 0.32 mmol) in anhydrous DCM (2 mL) was added dropwise over 10 min. The reaction was maintained at 0 °C for 30 min, then allowed to warm gradually to room temperature and stirred for 1.5 h. Upon completion, the reaction mixture was concentrated under reduced pressure The crude residue was purified by silica gel column chromatography (DCM/MeOH = 25/1) to afford 30-4b as an orange-red solid (121.00 mg, 85.8%). ^{1}H NMR (500 MHz, DMSO-d_6, δ): 10.42 (s, 1H), 10.21 (s, 1H), 9.48 (t, *J* = 6.2 Hz, 1H), 8.97 (s, 1H), 7.77 (d, *J* = 15.5 Hz, 1H), 7.54 (s, 1H), 7.31 (d, *J* = 8.7 Hz, 2H), 7.09 (s, 1H), 6.75 (d, *J* = 8.7 Hz, 2H), 6.46-6.39 (m, 1H), 6.28 (dd, *J* = 16.9, 2.0 Hz, 1H), 5.80 (dd, *J* = 9.9, 2.0 Hz, 1H), 4.72 (d, *J* = 6.1 Hz, 2H), 3.04 (t, *J* = 5.0 Hz, 4H), 2.42 (t, *J* = 4.9 Hz, 4H), 2.21 (s, 3H). LC-MS(ESI): m/z: 523.2$[M+H]^+$.

N-(3-(((5-amino-2-((4-(4-methylpiperazin-1-yl)phenyl)amino)pyrimidin-4-yl)amin o)methyl)-5-chlorophenyl)acrylamide (30-5b). To a solution of intermediate 30-4b (121.00 mg, 0.23 mmol) in ethanol (16 mL) and water (4 mL), iron powder (61.48 mg, 1.16 mmol) and ammonium chloride (122.96 mg, 2.32 mmol) was added. The reaction mixture was stirred at 90 °C for 2 hours. The reaction mixture was hot-filtered through diatomite and concentrated under reduced pressure. The residue was adjusted with saturated sodium bicarbonate solution to pH 9 and extracted with water and ethyl acetate, the combined organic layers were washed with saturated salt water, dried over anhydrous sodium sulfate, and concentrated to obtain a brown solid product 30-5b as a pale-yellow solid (92.50 mg, 61.4%) without further purification. LC-MS(ESI): m/z: 493.2$[M+H]^+$.

N-(3-chloro-5-((2-((4-(4-methylpiperazin-1-yl)phenyl)amino)-7-oxopteridin-8(7H)-yl)methyl)phenyl)acrylamide (30). To a solution of intermediate 30-5b (92.50 mg, 0.19 mmol) in ethanol (6 mL) and acetic acid (1 mL) was added 50% ethyl glyoxylate in toluene (76.7 mg, 0.38 mmol). The mixture was stirred at 90 °C under reflux. Upon completion, the mixture was concentrated under reduced pressure and adjusted to pH 9-10 with saturated $NaHCO_3$ and extracted with DCM (3×70 mL). The combined organic layers were washed with saturated brine, dried over anhydrous sodium sulfate and concentrated. Purification by silica gel column chromatography (DCM/MEOH = 15:1) to afforded 30 as an orange solid (58.32 mg, 27.8%).^{1}H NMR (500 MHz, DMSO-d_6, δ): 10.42 (s, 1H), 10.15 (s, 1H), 8.84 (s, 1H), 8.05 (s, 1H), 7.84 (s, 1H), 7.42 (s, 3H), 7.10 (s, 1H), 6.86 (d, *J* = 8.6 Hz, 2H), 6.40 (dd, *J* = 17.0, 10.1 Hz, 1H), 6.26 (dd, *J* = 17.0, 2.0 Hz, 1H), 5.78 (dd, *J* = 10.0, 2.0 Hz, 1H), 5.35 (s, 2H), 3.19 (s, 4H), 2.81 (s, 4H), 2.48 (s, 3H). HRMS (ESI) calculated for $C_{27}H_{27}ClN_8NaO_2[M+Na]^+$ = 553.1838, found 553.1847. HPLC purity: 96.39%, retention time: 4.274 min.

N-(3-fluoro-5-((2-((4-(4-methylpiperazin-1-yl)phenyl)amino)-7-oxopteridin-8(7H)-yl)methyl)phenyl)acrylamide (29). Compound 29 was synthesized according to the method of compound 30, orange solid with 14.3% yield.^{1}H NMR (500 MHz, DMSO-d_6, δ): 10.37 (s, 1H), 10.11 (s, 1H), 8.83 (s, 1H), 8.03 (s, 1H), 7.58 (d, *J* = 11.2 Hz, 1H), 7.38 (s, 2H), 7.31 (s, 1H), 6.88-6.72 (m, 3H), 6.38 (dd, *J* = 17.0, 10.0 Hz, 1H), 6.27 (dd, *J* = 17.0, 2.1 Hz, 1H), 5.79 (dd, *J* = 9.9, 2.1 Hz, 1H), 5.35 (s, 2H), 3.05 (t, *J* = 5.0 Hz, 4H), 2.45 (t, *J* = 5.0 Hz, 4H), 2.23 (s, 3H). HRMS (ESI) calculated for $C_{27}H_{27}FN_8NaO_2[M+Na]^+$ = 537.2133, found 537.2147. HPLC purity: 98.25%, retention time: 4.345 min.

N-(4-((2-((4-(4-methylpiperazin-1-yl)phenyl)amino)-7-oxopteridin-8(7H)-yl)methyl) pyridin-2-yl)acrylamide (31). Compound 31 was synthesized according to the method of compound 30, yellow solid with 12.9% yield. ^{1}H NMR (600 MHz, DMSO-d_6, δ): 10.80 (s, 1H), 10.10 (s, 1H), 8.84 (s, 1H), 8.30 (s, 1H), 8.21 (d, *J* = 5.2 Hz, 1H), 8.05 (s, 1H), 7.35 (s, 2H), 6.86 (s, 1H), 6.77 (s, 2H), 6.62 (dd, *J* = 17.0, 10.1 Hz, 1H), 6.32 (dd, *J* = 17.0, 2.0 Hz, 1H), 5.81 (d, *J* = 10.3 Hz, 1H), 5.41 (s, 2H), 3.03 (s, 4H), 2.46 (s, 4H), 2.25 (s, 3H). HRMS (ESI) calculated for $C_{26}H_{27}N_9NaO_2[M+Na]^+$ = 520.2180, found 520.2188. HPLC purity: 95.22%, retention time: 3.677 min.

Enzymatic Inhibition Assay

JAK kinase inhibitory activity and kinase family selectivity were assessed using the Z'-LYTE™ Kinase Assay Kit (Thermo Fisher Scientific) according to the manufacturer's instructions. The kinase activities of JAK1, JAK2, and JAK3 were tested using a kit with tyrosine 6 peptide as the peptide substrate, while TYK2 kinase activity was tested using a kit with tyrosine 3 peptide as the peptide substrate in a 384-well plate (Corning part number 3676). Briefly, the reaction mixture contains 5 μL of enzyme and the corresponding tyrosine peptide substrate (4 μM), and 2.5 μL of ATP (10 μM for JAK1, 25 μM for JAK2, 20 μM for JAK3 and 25 μM for TYK2). These components were pre-incubated with different concentrations of the compounds to be tested for 1 hour at room temperature. Color development reagents were then added to each well. After another 1 hour of incubation at room temperature, the color development reaction was terminated by the addition of a termination reagent. Fluorescence was measured at an excitation wavelength of 400 nm and emission wavelengths of 445/520 nm. Half-maximal inhibitory concentration (IC_{50}) values were calculated by curve fitting using GraphPad Prism 9.5 software.

Time-Dependent JAK3 inhibition assay with compound pre-incubation

Time-dependent JAK3 activity inhibition assays were performed using the

Z'-LYTE Kinase Assay Kit, with compounds pre-incubated with the JAK3 enzyme. Briefly, 2.5 μL of diluted JAK3 enzyme (from Active Motif) and 2.5 μL of test compound (at 4× the final concentration) were combined and incubated at room temperature for various durations (0, 8, 20, 30, 40, and 60 min). Subsequently, 5 μL of a reaction mixture containing 4 μM Peptide 6 and 10 μM ATP was added, and the mixture was further incubated at room temperature for 1 h. The final 10 μL kinase reaction mixture contained JAK3 enzyme, 5 μM ATP, and 2 μM Peptide 6 in kinase reaction buffer, with or without the test compound. Next, 5 μL of Development Reagent was added, and after a 1 h incubation at room temperature, the reaction was terminated by the addition of 5 μL of Stop reagent. Fluorescence signals were measured at an excitation wavelength of 400 nm and emission wavelengths of 445 nm and 520 nm. The inhibition rate was calculated according to the manufacturer's protocol.

Molecular Docking Study

Covalent docking experiments were performed using the Schrödinger Maestro software suite (Schrödinger LLC). The receptor template was the X-ray co-crystal structure of JAK3 in complex with the ligand N-(3-(((5-chloro-2-((2-methoxy-4-(4-methylpiperazin-1-yl)phenyl)amino)pyrimidin-4-yl)amino)methyl)phenyl)acrylamide (L9) (PDB ID: 4Z16, resolution = 2.90 Å), which was downloaded from the Protein Data Bank (PDB, https://www.rcsb.org/structure/4Z16).

Receptor preparation was conducted via the Protein Preparation Wizard: all water molecules, non-protein atoms, and the bound ligand L9 were removed from the structure; the protonation states of residues were adjusted using Epik and PROPKA at pH 7.4; missing amino acid side chains and loops were filled with Prime software to ensure structural integrity of the receptor.

Ligands were prepared using the LigPrep module within Maestro: possible ionization and tautomeric states of the ligands were generated at pH 7.4, and their 3D structures were optimized to meet the requirements of docking.

Covalent docking was performed using the Glide Covalent Docking plugin: based on the binding mode of L9 with JAK3 in the 4Z16 co-crystal structure, Cys909 was selected as the reactive residue; the reaction type was set to "Michael addition" to mimic the covalent bond formation between the electrophilic group of the ligand and the thiol group of Cys909. The docking grid box was centered on Cys909, enclosing all residues within a 14 Å radius to ensure coverage of key binding sites. Docking was carried out in standard precision (SP) mode with default parameters. The conformer with the highest docking score was selected for subsequent analysis, and ligand-receptor interactions were visualized using the PyMOL Molecular Graphics System (version 1.3, Schrödinger LLC).

Kinase Spectrum Analysis

Kinase profiling was performed on the KINOMEScan platform (www.discoverx.com). The compounds were screened at a concentration of 100 nM against a panel of 468 kinases. Test compounds were prepared as 40× stocks in 100% DMSO and directly diluted into the assay mixture. The results were defined as a percentage of the signal between the negative (DMSO, 100% control) and positive (control, 0% control) controls, which was calculated as follows: percent control = [(test compound signal − positive control signal)/(negative control signal − positive control signal)] × 100.

Pharmacokinetic Analysis

Male Sprague-Dawley rats (200-250 g) were randomly divided into two groups (n = 3 per group). A catheter was surgically placed in the femoral vein to collect blood samples. The rats were fasted overnight before dosing. Compound 15 was administered by intravenous injection or oral gavage at a dose of 1 mg/kg in a saline mixture (DMSO/PEG400/saline = 5:40:55) or 10 mg/kg in 0.5% methylcellulose, respectively. The plasma at each time point (5 min, 15 min, 30 min, 1 h, 2 h, 4 h, 6 h, 8 h, and 24 h) was collected in heparin tubes, and the compound concentrations were determined via LC–MS/MS. The LC system comprised a Waters (Waters Corporation, UAS) ultraperformance liquid chromatography (UPLC) instrument equipped with an ACQUITY UPLC binary solvent manager, ACQUITY UPLC autosampler module, ACQUTIY UPLC sample organizer, and ACQUITY UPLC column heater HT. Mass spectrometric analysis was performed via an API 5500 (triple quadrupole) instrument (Applied Biosystems/MDS Sciex) with an ESI source. The data acquisition and control system was created via Analyst 1.6.2 software from Applied Biosystems/MDS Sciex.).

Evaluation of the Effects of Compound 15 in Zebrafish Model of IBD

4 days post-fertilization (dpf) zebrafish larvae were randomly distributed into 6-well plates (30 embryos per well). The IBD model group was induced by immersion in 0.025% dextran sulfate sodium (DSS), while the treatment group received a combined administration of DSS and compound 15. The drug solutions were refreshed daily, and experimental outcomes were evaluated at 7dpf. To quantitatively evaluate neutrophil infiltration in the intestinal tract, transgenic zebrafish Tg (lyz: DsRed2) with fluorescently labeled neutrophils were pretreated with the experimental compounds and ten randomly selected zebrafish larvae were imaged and analyzed using a laser scanning confocal microscope. To assess zebrafish intestinal reactive oxygen species (ROS) levels, wild-type zebrafish were incubated with the fluorescent probe H2DCFDA (DCFH-DA) for 15 min at 28 °C after drug pretreatment, then were washed using PBS buffer and imaged with a confocal microscope. Fluorescence intensity was quantified using the LAXS software. For gene expression analysis, fifty zebrafish larvae pre-treated with drugs were homogenized using a tissue grinder. Total RNA was extracted using Trizol reagent and reverse-transcribed into cDNA with an RT SuperMix for qPCR kit. The primer sequences used for qPCR were shown in Table S3. The relative expression levels of target genes were normalized to the internal reference gene B-actinand calculated using the $2^{-\Delta\Delta CT}$ method. Experiments were performed in triplicate. Zebrafish were fixed in 4% paraformaldehyde, embedded in paraffin, sectioned at 5 μM, and stained with hematoxylin and eosin (H&E) for histopathological examination. Images were captured using a light microscope (Leica) at ×400 magnification.

Effects of Compound 15 or Tofacitinib on Zebrafish Platelets

Tg (CD41: EGFP) transgenic zebrafish embryos were cultured in 6-well plates with 30 embryos per well. At 2 dpf, the embryos were treated with the compound 15 or tofacitinib at a concentration of 5 μM, 50 μM, 500 μM for 48 hours, while the control group was treated with 0.1% DMSO. The solubility of compound 15 in zebrafish culture medium was assessed by HPLC (Figure S7). The 5 and 50 μM working solutions remained clear and fully dissolved, whereas the 500 μM solution appeared as a suspension. Following treatment, images of randomly selected zebrafish larvae were acquired on a laser scanning confocal microscope. The total fluorescence intensity of green-spotted platelets was analyzed using ImageJ software, and the measurement range of non-specific fluorescence regions near the yolk sac was excluded. Statistical analysis was performed using GraphPad Prism 8 via a one-way ANOVA test.

REFERENCES

1. Xue C., Yao Q., Gu X., et al. (2023). Evolving cognition of the JAK-STAT signaling pathway: autoimmune disorders and cancer. *Signal transduction and targeted therapy* **8**:204. DOI:10.1038/s41392-023-01468-7
2. Philips R. L., Wang Y., Cheon H., et al. (2022). The JAK-STAT pathway at 30:Much learned, much more to do. *Cell* **185**:3857–3876. DOI:10.1016/j.cell.2022.09.023
3. Hu Q., Bian Q., Rong D., et al. (2023). JAK/STAT pathway: Extracellular signals, diseases, immunity, and therapeutic regimens. *Frontiers in bioengineering and biotechnology* **11**:1110765. DOI:10.3389/fbioe.2023.1110765
4. Gadina M., Johnson C., Schwartz D., et al. (2018). Translational and clinical advances in JAK-STAT biology: The present and future of jakinibs. *Journal of leukocyte biology* **104**:499–514. DOI:10.1002/jlb.5ri0218-084r
5. Lv Y., Qi J., Babon J. J., et al. (2024). The JAK-STAT pathway: from structural biology to cytokine engineering. *Signal transduction and targeted therapy* **9**:221. DOI:10.1038/s41392-024-01934-w
6. Degryse S., de Bock C. E., Cox L., et al. (2014). JAK3 mutants transform hematopoietic cells through JAK1 activation, causing T-cell acute lymphoblastic leukemia in a mouse model. *Blood* **124**:3092–3100. DOI:10.1182/blood-2014-04-566687
7. Hu X., Li J., Fu M., et al. (2021). The JAK/STAT signaling pathway: from bench to clinic. *Signal transduction and targeted therapy* **6**:402. DOI:10.1038/s41392-021-00791-1
8. Banerjee S., Biehl A., Gadina M., et al. (2017). JAK-STAT Signaling as a Target for Inflammatory and Autoimmune Diseases: Current and Future Prospects. *Drugs* **77**:521–546. DOI:10.1007/s40265-017-0701-9

9. Bruner L. P., White A. M. and Proksell S. (2023). Inflammatory Bowel Disease. *Primary care* **50**:411–427. DOI:10.1016/j.pop.2023.03.009
10. Meštrović A., Kumric M. and Bozic J. (2024). Discontinuation of therapy in inflammatory bowel disease: Current views. *World journal of clinical cases* **12**:1718–1727. DOI:10.12998/wjcc.v12.i10.1718
11. Raine T., Bonovas S., Burisch J., et al. (2022). ECCO Guidelines on Therapeutics in Ulcerative Colitis: Medical Treatment. *Journal of Crohn's & colitis* **16**:2–17. DOI:10.1093/ecco-jcc/jjab178
12. Gordon H., Minozzi S., Kopylov U., et al. (2024). ECCO Guidelines on Therapeutics in Crohn's Disease: Medical Treatment. *Journal of Crohn's & colitis* **18**:1531–1555. DOI:10.1093/ecco-jcc/jjae091
13. Beaugerie L., Brousse N., Bouvier A. M., et al. (2009). Lymphoproliferative disorders in patients receiving thiopurines for inflammatory bowel disease: a prospective observational cohort study. *Lancet (London, England)* **374**:1617–1625. DOI:10.1016/s0140-6736(09)61302-7
14. Peyrin-Biroulet L., Khosrotehrani K., Carrat F., et al. (2011). Increased risk for nonmelanoma skin cancers in patients who receive thiopurines for inflammatory bowel disease. *Gastroenterology* **141**:1621-1628.e1621-1625. DOI:10.1053/j.gastro.2011.06.050.
15. Lopez A., Mounier M., Bouvier A. M., et al. (2014). Increased risk of acute myeloid leukemias and myelodysplastic syndromes in patients who received thiopurine treatment for inflammatory bowel disease. *Clinical gastroenterology and hepatology : the official clinical practice journal of the American Gastroenterological Association* **12**:1324–1329. DOI:10.1016/j.cgh.2014.02.026
16. Villarino A. V., Kanno Y. and O'Shea J. J. (2017). Mechanisms and consequences of Jak-STAT signaling in the immune system. *Nature immunology* **18**:374–384. DOI:10.1038/ni.3691
17. O'Shea J. J. and Plenge R. (2012). JAK and STAT signaling molecules in immunoregulation and immune-mediated disease. *Immunity* **36**:542–550. DOI:10.1016/j.immuni.2012.03.014
18. Roda G., Dal Buono A., Argollo M., et al. (2020). JAK selectivity: more precision less troubles. *Expert review of gastroenterology & hepatology* **14**:789–796. DOI:10.1080/17474124.2020.1780120
19. Gros B. and Kaplan G. G. (2023). Ulcerative Colitis in Adults: A Review. *Jama* **330**:951–965. DOI:10.1001/jama.2023.15389
20. Sandborn W. J., Su C. and Panes J. (2017). Tofacitinib as Induction and Maintenance Therapy for Ulcerative Colitis. *The New England journal of medicine* **377**:496–497. DOI:10.1056/NEJMc1707500
21. Grozovsky R., Begonja A. J., Liu K., et al. (2015). The Ashwell-Morell receptor regulates hepatic thrombopoietin production via JAK2-STAT3 signaling. *Nature Medicine* **21**:47–54. DOI:10.1038/nm.3770
22. Ytterberg S. R., Bhatt D. L., Mikuls T. R., et al. (2022). Cardiovascular and Cancer Risk with Tofacitinib in Rheumatoid Arthritis. *New England Journal of Medicine* **386**:316–326. DOI. DOI:10.1056/NEJMoa2109927
23. Wojciechowski J., Mukherjee A., Banfield C., et al. (2024). Model-Informed Assessment of Probability of Phase 3 Success for Ritlecitinib in Patients with Moderate-to-Severe Ulcerative Colitis. *Clinical pharmacology and therapeutics* **116**:724–735. DOI:10.1002/cpt.3251
24. Thorarensen A., Dowty M. E., Banker M. E., et al. (2017). Design of a Janus Kinase 3 (JAK3) Specific Inhibitor 1-((2S,5R)-5-((7H-Pyrrolo[2,3-d]pyrimidin-4-yl)amino)-2-methylpiperidin-1-yl)prop-2-en-1-one (PF-06651600) Allowing for the Interrogation of JAK3 Signaling in Humans. *Journal of medicinal chemistry* **60**:1971–1993. DOI:10.1021/acs.jmedchem.6b01694
25. Telliez J. B., Dowty M. E., Wang L., et al. (2016). Discovery of a JAK3-Selective Inhibitor: Functional Differentiation of JAK3-Selective Inhibition over pan-JAK or JAK1-Selective Inhibition. *ACS chemical biology* **11**:3442–3451. DOI:10.1021/acschembio.6b00677
26. Sandborn W. J., Danese S., Leszczyszyn J., et al. (2023). Oral Ritlecitinib and Brepocitinib for Moderate-to-Severe Ulcerative Colitis: Results From a Randomized, Phase 2b Study. *Clinical gastroenterology and hepatology : the official clinical practice journal of the American Gastroenterological Association* **21**:2616–2628.e2617. DOI:10.1016/j.cgh.2022.12.029
27. Li S., Si H., Song X., et al. (2022). Discovery of Hexahydrofuro[3,2-b]furans as New Kinase-Selective and Orally Bioavailable JAK3 Inhibitors for the Treatment of Leukemia Harboring a JAK3 Activating Mutant. *Journal of medicinal chemistry* **65**:10674–10690. DOI:10.1021/acs.jmedchem.2c00922
28. Chen C., Yin Y., Shi G., et al. (2022). A highly selective JAK3 inhibitor is developed for treating rheumatoid arthritis by suppressing γc cytokine–related JAK-STAT signal. *Science Advances* **8**:eabo4363. DOI. DOI:10.1126/sciadv.abo4363
29. Forster M., Chaikuad A., Bauer Silke M., et al. (2016). Selective JAK3 Inhibitors with a Covalent Reversible Binding Mode Targeting a New Induced Fit Binding Pocket. *Cell Chemical Biology* **23**:1335–1340. DOI:10.1016/j.chembiol.2016.10.008
30. Tian L., Li J., Yu J., et al. (2026). Covalent JAK3 inhibitors based on 2-arylamino and 7H-pyrrolo[2,3-d]pyrimidine scaffold: design, synthesis, and biological evaluation for the potential treatment of bortezomib-resistant multiple myeloma. *European Journal of Medicinal Chemistry* **310**:118764. DOI:https://doi.org/10.1016/j.ejmech.2026.118764.
31. Cui G., Li R., An D., et al. (2025). Design and Synthesis of Novel Dual Inhibitors for JAK3 and TEC Kinases in Autoimmune Disorders. *Journal of medicinal chemistry* **68**:13268–13294. DOI:10.1021/acs.jmedchem.4c02288
32. Hossain M. M., Khalid A., Akhter Z., et al. (2024). Discovery of a novel and highly selective JAK3 inhibitor as a potent hair growth promoter. *Journal of Translational Medicine* **22**:370. DOI:10.1186/s12967-024-05144-4
33. Tan L., Akahane K., McNally R., et al. (2015). Development of Selective Covalent Janus Kinase 3 Inhibitors. *Journal of medicinal chemistry* **58**:6589–6606. DOI:10.1021/acs.jmedchem.5b00710
34. Goedken E. R., Argiriadi M. A., Banach D. L., et al. (2015). Tricyclic covalent inhibitors selectively target Jak3 through an active site thiol. *The Journal of biological chemistry* **290**:4573–4589. DOI:10.1074/jbc.M114.595181
35. Talasila S., Lee E., Teichner E. M., et al. (2024). Analysis of publicly available adverse events reported for pediatric patients treated with Janus kinase inhibitors. *Pediatric Dermatology* **41**:1040-1046. DOI:https://doi.org/10.1111/pde.15721.
36. Kadoba K., Waki D., Nishimura K., et al. (2020). Development of severe thrombocytopenia with TAFRO syndrome-like features in a patient with rheumatoid arthritis treated with a Janus kinase inhibitor: A case report. *Medicine* **99**:e22793. DOI:10.1097/md.0000000000022793

FUNDING AND ACKNOWLEDGMENTS

This work was supported in part by the National Natural Science Foundation of China (82425104), the National Key R&D Program of China (2022YFC3400501, 2022YFC3400504). The funders had no role in study design, data collection and analysis, decision to publish, or preparation of the manuscript.

AUTHOR CONTRIBUTIONS

C.W., C.H. and Y.W. were co-first authors and contributed equally to this work. The manuscript was written through contributions of all authors. All authors have given approval to the final version of the manuscript.

DECLARATION OF INTERESTS

Honglin Li is an Editorial Board member of The Innovation Drug Discovery and was blinded from reviewing or making final decisions on the manuscript. Peer review was handled independently of this member and their research group. The other authors declare no conflicts of interest.

SUPPLEMENTAL INFORMATION

It can be found online at https://doi.org/10.59717/j.xinn-drugdisc.2026.100029.